

**Supplementary Information to accompany**  
**“Biogeochemical significance of Ecosystem Function:**  
**An end-Cretaceous Case Study”**

by

**Michael J. Henehan, Pincelli M. Hull, Donald E. Penman, James W.  
B. Rae and Daniela N. Schmidt.**

**Contents, Supplementary Methods and Discussion**

1. Data Overview (p. 1)
2. Age models (p. 1-3)
  - a. Age Models: IODP Sites 1267 & 1209 (p. 1-2)
  - b. Age Models: Previously published data (p. 2-3)
3. Preservation indices (p. 3-6)
4. Record from DSDP 525 (p. 6)
5. LOSCAR
  - a. Configurations and boundary conditions (p. 7)
  - b. Deccan Trap simulations: Fluxes and Timescales (p. 7-10)
  - c. Deccan Trap simulations: Avoiding a Carbonate Overshoot (p. 10-12)
  - d. K-Pg bolide aftermath (p. 14-16)
6. Literature cited (p. 16-24)

**Supplementary Figures:**

- Fig. S1 Planktic Foraminiferal Fragmentation (p. 4)  
Fig. S2 IODP Site U1403 Foram preservation (p. 5)  
Fig. S3 Dissolution Susceptible Coccolithophores (p. 5)  
Fig. S4 Records of Fragmentation from DSDP Site 525 (p. 6)  
Fig. S5 Surface water saturation changes (p. 8)  
Fig. S6 Rate of eruption (p. 9)  
Fig. S7 Pulsed emission scenario (p. 10)  
Fig. S8 Compensating for carbonate overshoot: Changing CaCO<sub>3</sub>:C<sub>org</sub> ratio (p. 12)  
Fig. S9 Compensating for carbonate overshoot: Shelf sedimentation (p. 13)  
Fig. S10 Effect of different silicate weathering feedback strengths (p. 13)  
Fig. S11 Effect of different CaCO<sub>3</sub> flux decreases at the K-Pg boundary (p. 15)

**1. Data Overview**

This manuscript collates a large range of both new and published proxy records, including of ocean temperature, carbonate preservation and <sup>187</sup>Os/<sup>188</sup>Os. Plotted records of carbonate preservation are:

- Published weight percent (wt. %) CaCO<sub>3</sub> data from ODP 690[1–3] and IODP U1403[4].
- New records of planktic foraminiferal fragmentation from ODP Sites 1209 and 1267, and published planktic foraminiferal fragmentation records from DSDP 527[5], DSDP 528[6], DSDP 577[6], and ODP 1209[7].
- Published records of planktic foraminifera per gram from DSDP Site 577[8].
- New records of wt. % coarse fraction from IODP U1403 (> 38 μm) and ODP 1267 (> 63 μm), with published records from DSDP 577[9], ODP 1209[10], ODP 1262[10].

Temperature records are all published δ<sup>18</sup>O data, from ODP 1209[11], DSDP 525[12], DSDP 528[13] and ODP 690[14]. <sup>187</sup>Os/<sup>188</sup>Os data are from [2].

**2. Age Models**

**2a. Age Models: ODP Sites 1267 & 1209**

New foraminiferal fragmentation counts were collected on 132 samples (80 at ODP 1209, 52 at ODP 1267; Table S2-S3). The two sites, ODP Site 1267 (28.098° S, 1.711° E, Walvis Ridge, South-East

Atlantic) and ODP Site 1209 (32.652° N, 158.506° E, Shatsky Rise, North-West Pacific) are the best-studied K-Pg locations in scientific drilling due to the recovery of well-preserved, complete boundaries[15,16] and the subsequent development of cyclostratigraphic age models[11,17–19]. The K-Pg boundary interval at both sites comprises calcareous nannofossil carbonate oozes, with a higher wt. % CaCO<sub>3</sub> at Site 1209 as compared to Site 1267 during this interval (typically > 96 % versus the more variable 55 - 95 %). Sediment samples from Site 1267 ranged in colour from red to clay-brown while at Site 1209 samples were whiter in colour[15,16].

The most recent cyclostratigraphic age models for Walvis Ridge, and other K-Pg sites, is from Westerhold et al.[19]. In Westerhold et al.[19], only Walvis Ridge Site 1262 was tuned, and not our focal site, Site 1267. In order to use the most recent age model from Westerhold et al.[19] (Age Option 3, allowing for best agreement with GTS2012[20]), previously published tie-points between Site 1262 and Site 1267 (Tables S5 and S6, Westerhold et al.[18]) were used to transfer the more recent age model to Site 1267 via linear interpolation. The age assigned to the onset of C29r using these translated astronomical data is 66.405 Ma: in good agreement with the date of 66.398 Ma from GTS2012[20]. A similar procedure was used to translate the dated age points from Site 1262[19] to ODP Site 1209 using the tie points from Westerhold et al.[18] According to these age models, our sampling spans 607 kyr at ODP 1267 (~11 kyr resolution) and 428 kyr at ODP 1209 (~ 5kyr resolution).

## **2b. Age Models: Previously published data**

- a) **ODP Site 1209 (32° 39.10'N, 158° 30.36'E, Shatsky Rise, Pacific[16])**. Temperatures, as derived from benthic foraminiferal  $\delta^{18}\text{O}$ , are replotted from Westerhold et al.[11] in Fig 1b, with an age model constructed as in Section 1a above. Wt. % Sand Fraction from the same study is plotted in Fig. 2, Panel a.
- b) **ODP Site 690 (65°9.629'S, 1°12.296'E, Maud Rise, Southern Ocean[21])**. At this site we combine existing records of Os isotopes from Robinson et al.[2] (Fig. 1a), temperature (derived from bulk  $\delta^{18}\text{O}$  from Stott and Kennett[14] using Erez and Luz[22] for consistency with ref. [[11]]; Fig. 1b) and wt. % CaCO<sub>3</sub> from Ehrendorfer[1], Robinson et al.[2], and O'Connell[3] (Fig 1c). A unified age model for these data was constructed based on interpolation between documented magnetochron boundaries[23] (assigning absolute chron boundary ages according to GTS2012[20]) and the position of the K-Pg Ir spike[24].
- c) **DSDP Site 577 (32°26.51'N, 157°43.40'E, Shatsky Rise, Pacific[25])**. Four existing records were used from DSDP Site 577. Wt. % CaCO<sub>3</sub>, Wt. % Sand Fraction and foraminiferal fragmentation data (Fig. 2) are from Zachos et al.[9,26] and D'Hondt[6]. Counts of planktic foraminiferal abundance (Fig. 1h) are from Gerstel et al.[8]. Os isotope data are from Robinson et al.[2] and references therein (Fig. 1a). The age models for these data (Fig. 1-2) use the revised composite depth scale of Dickens and Backman.[27]. For consistency with other sites, we derive absolute ages from documented magnetochron boundaries[28] and the position of the K-Pg boundary[25] (dated as per GTS2012[20]). Note that for DSDP 577\*, used in ref.[[8]], there is no magnetochron boundary or nannofossil FAD below the C29r/C30n boundary: drilling ceased within the *M. murus* biozone (in Chron 30n). In the absence of better age constraints, in Fig. 1h we extend the sedimentation rate from between the K-Pg and the C29r/C30n reversal through Chron 30n. In recognition of this poor age constraint, we denote data with extrapolated ages with a dashed line, and suggest that the apparent mismatch between the onset of dissolution at this site compared to both nearby Site 1209 and elsewhere, may be the result of poor temporal constraints during Chron 30n at DSDP Site 577\*.
- d) **DSDP Site 525 (29°04.24'S, 02°59.12'E, Walvis Ridge, South Atlantic[25])**. Os isotope data from Robinson et al.[2] (Fig. 1a) and temperatures from Li and Keller[12] are re-assigned ages according to GTS2012 dates[20] for the K-Pg, C30n/C29r, and C30r/C30n boundaries[from 29]. Temperature for DSDP 525 is derived from benthic foraminiferal  $\delta^{18}\text{O}$  using Erez and Luz[22] for consistency with ref. [[11]] (Fig 1b). However, note that we propose that the placement of the C30n/C29r boundary at DSDP 525[29] may be incorrect (as discussed in Section 4).
- e) **DSDP Site 527 (28°02.49'S, 01°45.80'E, Walvis Ridge, South Atlantic[25])** Foraminiferal fragmentation and wt. % CaCO<sub>3</sub> data (Figs. 1 & 2) are taken from Kucera et al.[5] The age model for this site is constructed based on documented magnetochron boundaries[29] and the position of the K-Pg boundary (dated as per GTS2012[20]).
- f) **DSDP Site 528 (28°31.49'S, 02°19.44'E, Walvis Ridge, South Atlantic[25])**. Foraminiferal fragmentation and wt. % CaCO<sub>3</sub> data are taken from D'Hondt[6]. Temperature for DSDP 528 is

derived from D'Hondt and Lindiger[13] using Erez and Luz[22] for consistency with ref. [[11]] (Fig1b). The age model for this site is constructed based on documented magnetochron boundaries[29] and the position of the K-Pg boundary (dated as per GTS2012[20]).

- g) **ODP Site 1262**. Percent sand fraction data are from Mastersizer analyses in Hull et al.[10], with age model updated to that of Westerhold et al.[19] (see also section 2a).
- h) **Bottacione Gorge (43°21.77'N, 12° 34.96'E, Tethys[30])**. Os isotope data from Robinson et al.[2] (Fig. 1a) are re-assigned ages according to GTS2012[20] dates for the K-Pg, C30n/C29r, and C30r/C30n boundaries from ref. [[31]], as cited in ref. [[2]].
- i) **IODP Site U1403 (39°56.60'N, 51°48.20'W, North Atlantic[4])**. Preliminary shipboard CaCO<sub>3</sub> measurements are dated according to the average depths of nannofossil first appearance datums (FADs) for *M. prinsii* and *M. murus*[4]. Although the date assigned as FAD for *M. prinsii* is 67.3 Ma (following GTS2012[20]), we note that the appearance of this taxa is probably diachronous[32], with the lowest occurrence of *M. prinsii* at open ocean sites almost always occurring just above the onset of magnetochron C29r (e.g. at Sites 356, 384, 516, 525, 527, 548, 1262 in the Atlantic Ocean, and Sites 465 and 577 in the Pacific Ocean[15,32,33]). Therefore we use Henriksson's[32] North Atlantic FAD for *M. prinsii* of 0.22 Ma before the K-Pg boundary.

### 3. Preservational indicators

Here we use a number of different preservational indices to detect changes in deep ocean carbonate saturation, according to data availability and suitability. Each measure has associated strengths and weaknesses, which we detail here.

**Planktic Foraminiferal Fragmentation:** The degree of fragmentation of foraminiferal tests has long been used as an indicator of carbonate saturation state[e.g. 34,35–38]. Compared to other indicators, such as wt. % CaCO<sub>3</sub>, or wt. % Coarse Fraction, it has the benefit of being independent of changes in productivity or export of nanoplankton and foraminifera, or changes in terrestrial input. Also, at sites where there is very little delivery of terrigenous material or silica to the seafloor (e.g. Shatsky Rise), only severe changes in carbonate preservation are likely to significantly alter the wt. % CaCO<sub>3</sub>, as virtually all of the sediment is CaCO<sub>3</sub>. Moderate changes in carbonate preservation at such sites might still, however, have a noticeable effect on i) the ratio of micro to nanno-fossils due to their relative corrosion resistance, and ii) on the ratio of intact to fragmented foraminiferal tests. In this way, changes in planktic foraminiferal fragmentation resolve finer-scale changes in ocean saturation at sites like Shatsky Rise, and therefore may often prove most adept at detecting past events (as is shown during the PETM[39]). One drawback of the proxy, however, is that at shallower depths (<~500m), fragmentation may be only loosely correlated with ocean saturation state (as is the case in the modern ocean; see **Fig. S1**), with delivery of organic matter and strength of local currents often exerting an important influence[e.g. 40,41]. Also, methods used for classifying and counting fragments vary[36,42], which can result in offsets in absolute values between datasets, even if slopes of fragmentation change vs. saturation in different studies may be strikingly similar (Fig. S1). It is for this reason that we make no attempt to normalise each study's fragmentation count data in Fig. 1 to make metrics consistent across sites. Here, to avoid subjectivity over what constitutes a foraminiferal 'fragment', from whence much of the inconsistencies between datasets probably arises, we count the relative abundance of 'complete' tests for the two new datasets from ODP Sites 1209 and 1267 (i.e. whole tests that have no detectable signs of any breakage or dissolution of chambers). Samples (>125 µm size fraction) were split repeatedly to obtain a small but statistically representative sample size (200 - 400 tests) for counting. Samples from Site U1403 were lacking in Maastrichtian planktic foraminifera, as a result of near-complete dissolution of planktonic foraminifera, so no fragmentation counts were possible. Representative samples were imaged as per ref. [[43]], and are shown in **Fig. S2** instead.

**Weight Percent (wt. %) CaCO<sub>3</sub>:** Where no data for planktic foraminiferal fragmentation were available, we compiled existing wt. % CaCO<sub>3</sub> or wt. % coarse fraction when available. Although in most circumstances this metric should reflect the degree of dissolution of carbonates at the seafloor[39,44], it is also sensitive to changes in terrestrial input and export fluxes[39], and may also be complicated by micrite recrystallization and secondary calcite growth within sediments[e.g. 8]. In addition, the relative abundance of foraminifera compared to coccolithophores can affect the use of wt. % CaCO<sub>3</sub> as a proxy to discern changes in deep ocean saturation. Because coccoliths are more resistant to dissolution than planktic foraminifera[e.g. 45], a site with very low foraminiferal abundance relative to coccoliths may require a larger change in saturation state to discernibly change wt. % CaCO<sub>3</sub>.

Therefore for sites like Shatsky Rise, foraminiferal fragmentation may be a more sensitive indicator, able to pick up more minor changes in carbonate saturation state.

*Weight Percent Coarse Fraction/Planktic foraminifera per cm<sup>3</sup>*. Similarly, wt. % coarse fraction has been used to indicate preservation[e.g. 46], due to preferential dissolution of foraminifera over nannofossils[e.g. 45], but as with wt. % CaCO<sub>3</sub> it does not always only reflect preservation[39], and can reflect changes in delivery of fine material, independent of saturation state. In the case of the K-Pg boundary, it is likely that the signal is primarily a manifestation of the collapse of the nannoplankton export and production[e.g. 6] and increased foraminiferal production[47], but that enhanced saturation state would have also played a role. Note that similarly high relative abundance of wt. % coarse fraction after the K-Pg is also observed at DSDP Site 47.2[48], but is not plotted here due to relatively poor age constraints. At DSDP 577\*, the number of planktic foraminifera per cm<sup>3</sup> is used as a metric for dissolution[8] prior to the K-Pg (Fig. 1h), which, as with wt. % coarse fraction, is built upon the preferential dissolution of planktic foraminifera relative to benthic foraminifera and coccoliths.

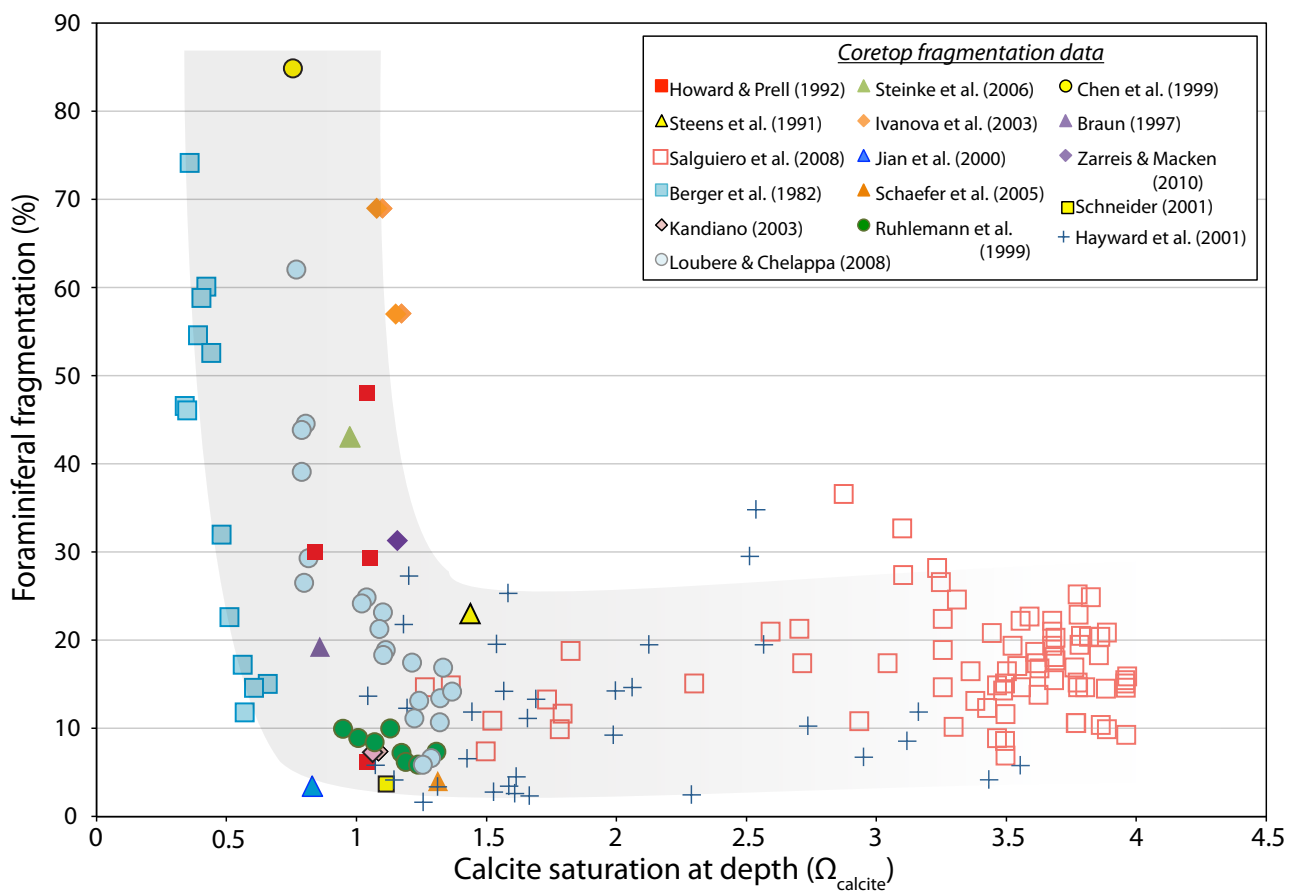


**Figure S1:** A compilation of published foraminiferal fragmentation counts in core-top sediments[36,40,41,46–58] is plotted against carbonate saturation state, as calculated via[refs. 59,60]. While there is considerable scatter in these records (likely in part due to methodological differences), there is good agreement in slopes of  $\Omega$ -Fragmentation curves within the foraminiferal lysocline ( $\Omega < \sim 1$ ).

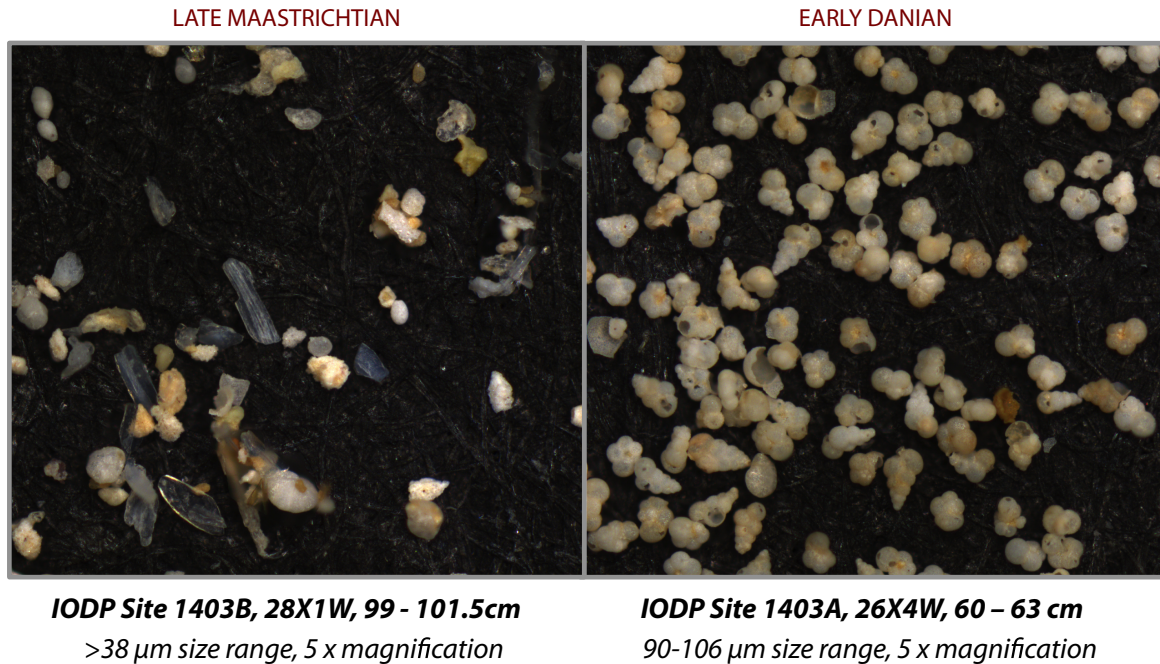


**Figure S2:** A comparison of typical foraminiferal preservation across the K-Pg boundary at IODP Site U1403. In the upper Maastrichtian sample (left), planktic foraminifera are not found, with only (often fragmented) benthic foraminifera preserved. In the Danian, however, planktic foraminifera are abundant, with even small foraminifera like those shown here (right) largely intact.

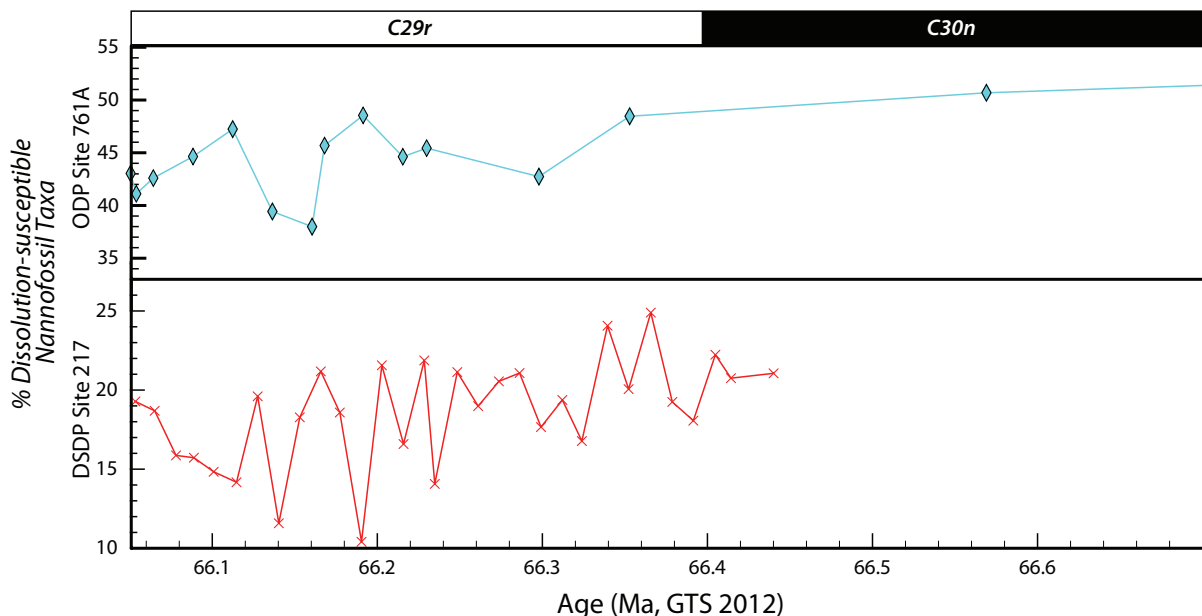


**Figure S3:** Abundances of dissolution-susceptible coccolithophores reproduced from Ehrendorfer[1], adjusted to the GTS2012 timescale[20]. Decreases in abundance appear to coincide with dissolution pulses seen elsewhere (Fig. 1), and may add further evidence for lysocline shoaling in the Maastrichtian

***Dissolution-susceptible coccolithophores:*** Amongst the nannofossils, not all species are equally dissolution prone: Theirstein[49] ranked species of Maastrichtian and Danian coccolithophores in order of dissolution susceptibility, based on acidification experiments. As a result, it is possible to draw some qualitative insight into carbonate saturation state based on preferential preservation of dissolution resistant coccoliths, providing there are no ecological range shifts at play. One such study is that of Ehrendorfer[1], which yielded a pattern of reduced relative abundance of dissolution prone coccoliths after the onset of C29r. Here we plot these data with an updated age model for consistency (**Fig. S3**). These data suggest similar patterns of lysocline shoaling following the onset of Deccan volcanism. Many of the species of coccoliths that are dominant in early Palaeocene sediments are highly dissolution prone: species such as *Cruciplacolithus primus* (by far the most dissolution susceptible of all Danian coccoliths tested) and *Zygodiscus sigmoides*. That these are so abundant in Danian deep sea sediments[50] may add further support to the idea that the ocean's carbonate saturation state was elevated in the early Danian.

#### 4. DSDP Site 525

In Fig. 1f fragmentation counts from DSDP Site 527[5] are plotted. However, Kucera et al.[5] also provided records from nearby site DSDP 525 and from DSDP Site 516 (Rio Grande Rise). We do not consider their record of fragmentation from DSDP 516 here, as the authors suggest the site is so far below the regional lysocline as to be uninformative. Both DSDP Site 527 and DSDP Site 525 show considerable variation in foraminiferal fragmentation (**Fig. S4**). The difference in the relative timing of increased fragmentation (roughly 100 kyr) between sites 525 and 527 was originally interpreted as reflecting regional currents[5]. However, here we suggest that the placement of the C30n/C29r boundary[29] used to construct the original age model for DSDP Site 525 may have been incorrect, and that these drops in fragmentation are in fact synchronous. There are several lines of evidence to support this assertion, besides the similarity in foraminiferal fragmentation patterns. Firstly, Os isotope ratios begin to trend towards lower values at Site 525 during Chron 30n, well before other sites with measured osmium isotopes. The short residence of Os in oceans (10-40kyr)[51] suggests Os isotopes should be uniform throughout the ocean, as is supported by synchronous declines in osmium isotopes at the C29r/C30n boundary at other geographically-disparate sites in the Tethys, Weddell Sea, and Pacific[2]. While it remains possible that there is some source of local heterogeneity in marine Os reservoir[2], a mis-assigned Chron boundary is perhaps more straightforward explanation for this phenomenon. Secondly, over this interval there is some evidence for reducing conditions within sediments, including green hue from ferrous iron and unusual concentrations of Re (G. Ravizza, pers. comm.), which could easily have contributed to spurious magnetochron assignments[52]. Finally, the diachronous first appearances of *Micula murus* across nearby DSDP Leg 86 Sites[53] could also result, at least in part, from compromised magnetostratigraphic dating rather than true diachroneity.

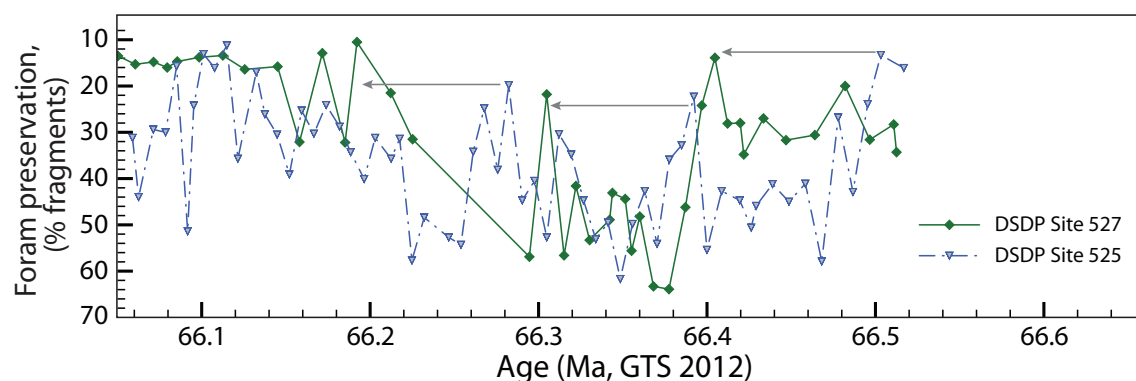


**Fig S4:** Records of fragmentation at DSDP Site 525 from Kucera et al.<sup>5</sup> show an increase in foraminiferal fragmentation around the time of other preservation signals. However, we note that the records appear offset from those at nearby DSDP 527, which we suggest is the result of incorrect placement of the onset of C29r in this core. Tentative tie points in the two fragmentation records are suggested as grey arrows.

## 5. LOSCAR

### 5a. Configurations and boundary conditions

Here we detail the modifications made to the 'PALEO' configuration of the geochemical box model LOSCAR (Long-term Ocean Sediment Carbon Reservoir)[54,55] version 2.0.4, in order to evaluate the impacts of volcanic degassing and calcifier extinction on the global carbon cycle.

In calculations of carbonate chemistry in ancient seawater, concentrations of  $\text{Ca}^{2+}$  and  $\text{Mg}^{2+}$  can have significant effects, due to ion pairing effects on equilibrium constants[56]. This is particularly true for the dissociation constants of carbonic acid and the solubility constants for calcite and aragonite. End-Cretaceous seawater likely had a much higher  $[\text{Ca}^{2+}]$  (~42 mmol/kg) and lower  $[\text{Mg}^{2+}]$  (~20 mmol/kg) [e.g. 57] than modern seawater ( $[\text{Ca}^{2+}] = 10.3$  mmol/kg;  $[\text{Mg}^{2+}] = 52.8$  mmol/kg). The equilibrium constants in LOSCAR must be corrected to account for this difference, in order to produce realistic carbonate chemistry calculations. Like most reconstructions of deep-time carbonate chemistry, LOSCAR v.2.0.4 uses the  $[\text{Ca}^{2+}]$  and  $[\text{Mg}^{2+}]$  correction factors of Ben-Yaakov & Goldhaber[56], which are likely suitable for smaller deviations of  $[\text{Ca}^{2+}]$  and  $[\text{Mg}^{2+}]$  from modern (e.g. the Eocene) but that are likely to prove inaccurate under much more divergent Cretaceous conditions[58]. Indeed, we found LOSCAR produced an unusual steady-state carbonate system configuration for Cretaceous conditions using this standard Mg and Ca corrections- namely, very low seawater DIC and alkalinity at steady state. Unlike previous methods which apply corrections to modern stoichiometric equilibrium constants, MyAMI builds thermodynamic equilibrium constants accounting for the activities of all ions in solution using the larger and more up-to-date MIAMI database[59]. We therefore reconfigured LOSCAR to perform carbonate chemistry calculations using the equilibrium constants provided by MyAMI[58] assuming  $[\text{Ca}^{2+}] = 42$  mmol/kg and  $[\text{Mg}^{2+}] = 20$  mmol/kg. This configuration produced equilibrium DIC and alkalinity values closer to modern conditions, in agreement with predictions[60]. While we acknowledge there is a degree of uncertainty on these reconstructed values of  $[\text{Ca}^{2+}]$  and  $[\text{Mg}^{2+}]$ , the effect of a few mmol difference in either parameter has no substantial influence on the conclusions drawn. In addition to adjusting equilibrium constants, we modelled at higher depth resolution (one sediment level every 100m, rather than the standard 500m) to better resolve deep-water carbonate dissolution and compensation depth.

On timescales suggested for total Deccan emplacement (100s of kyr[2,61,62, and references therein]) the weathering of silicate rocks (and subsequent carbonate burial) is the most important feedback for restoring equilibrium and drawing down  $\text{CO}_2$  following a perturbation to the carbon cycle. During Deccan volcanism silicate weathering is estimated to have been quite high due to the presence of large expanses of exposed Deccan basalt at low latitudes[63]. The silicate weathering feedback is parameterized in LOSCAR as:

$$F_{\text{si}} = F_{\text{eq,si}} * ([\text{CO}_2]_{\text{atm}} / [\text{CO}_2]_{\text{eq}})^{N_{\text{si}}}$$

where  $F_{\text{eq}}$  and  $[\text{CO}_2]_{\text{eq}}$  are equilibrium weathering flux and atmospheric  $\text{pCO}_2$  at which volcanic carbon emissions are perfectly balanced by silicate weathering and subsequent carbonate burial. The exponent  $N_{\text{si}}$  is a free parameter in the model that sets the strength of the silicate weathering feedbacks (default  $N_{\text{si}} = 0.2$ ,  $N_{\text{cc}} = 0.4$ ). Uchikawa and Zeebe[64] studied behaviour of LOSCAR using a range of  $N_{\text{si}}$  values; for runs plotted in Fig. 3 we use the highest weathering feedback strength considered by that study ( $N_{\text{si}} = 0.6$ ), on the basis that the abundance of freshly-exposed basalts at the equator during Deccan trap emplacement would have been readily weathered[65]. Lower values of  $N_{\text{si}}$  (0.05-0.4) less easily reproduced the temporal trajectory of the warming event in the latest Maastrichtian.

$\text{SO}_2$  degassing from LIP volcanism is thought to be converted to sulphuric acid ( $\text{H}_2\text{SO}_4$ ) before being rained out onto the Earth's surface. The portion falling on the ocean would have rapidly dissociated to sulphate anion ( $\text{SO}_4^{2-}$ ). This addition of an anionic salt reduces the negative charge deficit of the conservative salts, i.e. total alkalinity (TA). Since neither sulphur nor sulphate is explicitly modelled as a tracer in LOSCAR, we simulate the acidification of the oceans through sulphate addition by prescribing an equivalent reduction (2 mol for every mol S, as sulphate is a doubly charged anion) in total alkalinity (which is a tracer in LOSCAR). This TA reduction is applied to the surface ocean reservoirs only, but is subsequently mixed throughout the ocean due to vertical mixing and thermohaline circulation. A similar approach was taken by Tyrrell et al.[66] when modelling the influx of bolide-derived  $\text{SO}_2$  release at the K-Pg boundary.

### 5b. Deccan Trap simulations: Fluxes and Timescales

The onset of large scale flood basalt volcanism (the Deccan LIP) is thought to have released 4,000 - 9,500 gigatonnes of carbon (Gt C), with associated  $\text{SO}_2$  release[67], thereby far exceeding total anthropogenic  $\text{CO}_2$  emissions to date[68] but on the low end of potential fossil fuel resources (~8,500-13,600 GtC[69]). Unlike the ongoing anthropogenic experiment, however, cumulative Deccan

emissions were spread over a relatively long (>~100 kyr) timescale [62,67]. For simulations of Deccan degassing plotted in Fig. 3 of the main text, minimum and maximum emission scenarios (total CO<sub>2</sub> = 4,090 or 9,500 Gt C, total SO<sub>2</sub> = 3,200 or 8,500 Gt S[67]) were partitioned into two discrete pulses, in accordance with the proposed second and third stages of volcanism from Chenet et al.[61], and the eruptive volumes of Self et al.[70]: 86.5% of degassing over a ~140kyr interval beginning at the C30n/C29r reversal (corresponding to decreasing <sup>187</sup>Os/<sup>188</sup>Os[2]), and the second 13.5% at the end of C29r in the Danian. Most other estimates of CO<sub>2</sub> release for the Deccan Traps[71–74] are within the range of emissions assumed here[67]. CO<sub>2</sub>-only and SO<sub>2</sub>-only simulations were also carried out to more clearly distinguish the effects of both drivers. SO<sub>2</sub> release acts to acidify the ocean, causing a reduction in surface (Fig. S5) and deepwater (Fig. 3b) saturation state, surface pH (Fig. S5) and a release of CO<sub>2</sub> from the surface ocean (Fig. 3a) by altering the speciation of DIC. LOSCAR simulations of SO<sub>2</sub> release differ from CO<sub>2</sub> release scenarios by prompting a less pronounced ‘carbonate overshoot’ (see Section 6c) following acidification (Fig. 3b). In this way emission scenarios of a high-end SO<sub>2</sub> release but low-end CO<sub>2</sub> might better explain the lack of any increase in carbonate saturation indicated in sedimentary records (Fig. 1), but to achieve a warming of 2–3 °C such low end CO<sub>2</sub> release would necessitate either an unlikely end-Cretaceous climate sensitivity (~9 °C/CO<sub>2</sub> doubling), or equally unlikely low starting pCO<sub>2</sub> (~200 ppmv). Moreover, these scenarios do not consider the potential for antagonistic global cooling effects (although shorter-term) from SO<sub>2</sub> aerosols, if the pāhoehoe-type basaltic Deccan eruptions somehow reached the stratosphere[72,75], which could exacerbate this dilemma. Therefore our model results favour high levels of CO<sub>2</sub> release accompanying SO<sub>2</sub> release. We note that the maximum SO<sub>2</sub> and CO<sub>2</sub> emissions scenario shown in Fig. 3 produces similar patterns in atmospheric pCO<sub>2</sub> change to those estimated from palaeosol carbonates[76]. However, an outstanding issue is the mismatch between modelled patterns of sediment dissolution and our sedimentary records, with sediments suggesting much longer timescales of dissolution than models predict, which we discuss in Section 6c.

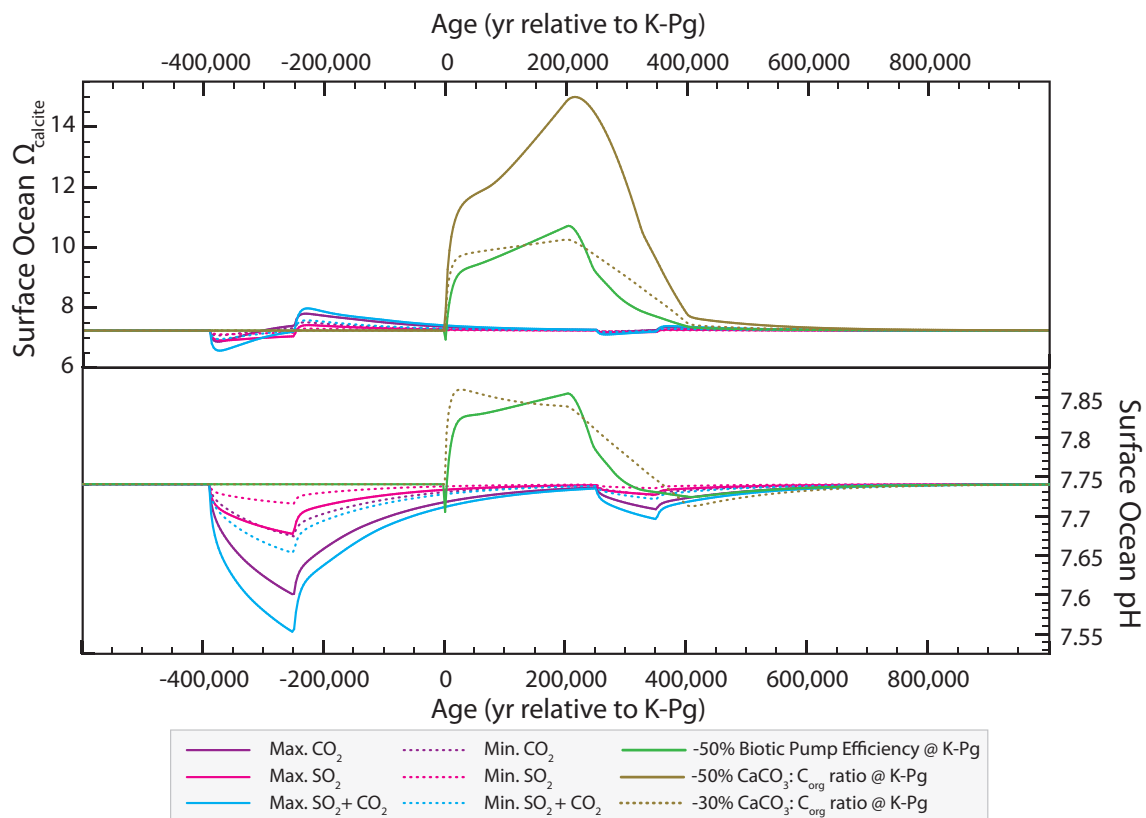


**Fig S5:** Surface ocean calcite saturation state and pH changes in response to LOSCAR simulations illustrated in Fig. 3. As is clear, very little reduction in surface ocean saturation state is predicted via even maximum Deccan emissions scenarios, in spite of large pH changes. However very large changes in both pH and saturation state are predicted in the face of removal of pelagic CaCO<sub>3</sub> producers at the K-Pg boundary.

The issue of rate of volcanic degassing is also critical. As shown in **Fig. S6**, erupting the maximum estimates of SO<sub>2</sub> and CO<sub>2</sub> release over timescales of < 100 kyr causes much more pronounced initial carbonate dissolution (and so would at first glance seem more compatible with observed carbonate dissolution). However, such rapid CO<sub>2</sub> rise would require unusually low climate sensitivity to be compatible with only a 2 - 3°C temperature rise. Moreover, these short timescales would still struggle to sustain dissolution (and to a lesser extent warming) for long enough to be compatible with observations from sediments over the last few hundred kyr of the Maastrichtian (Fig. 1). Finally, δ<sup>18</sup>O records (where data are high enough resolution; e.g. ODP Site 1209[11], and DSDP Site 525[12]) do not show the pronounced ‘sawtooth’ trajectory one would expect from an eruptive timescale of <100 kyr. Conversely, with eruptive scenarios of > 300 kyr, even with high-end weathering feedbacks used here (N<sub>SI</sub> = 0.6), it is difficult to reproduce the necessary drawdown of CO<sub>2</sub> before the K-Pg boundary implied by return to pre-event temperatures (Fig. 1). Therefore a timescale of ~140 kyr, as also implied by the window of declining <sup>187</sup>Os/<sup>188</sup>Os[2], seems most consistent with proxy observations.

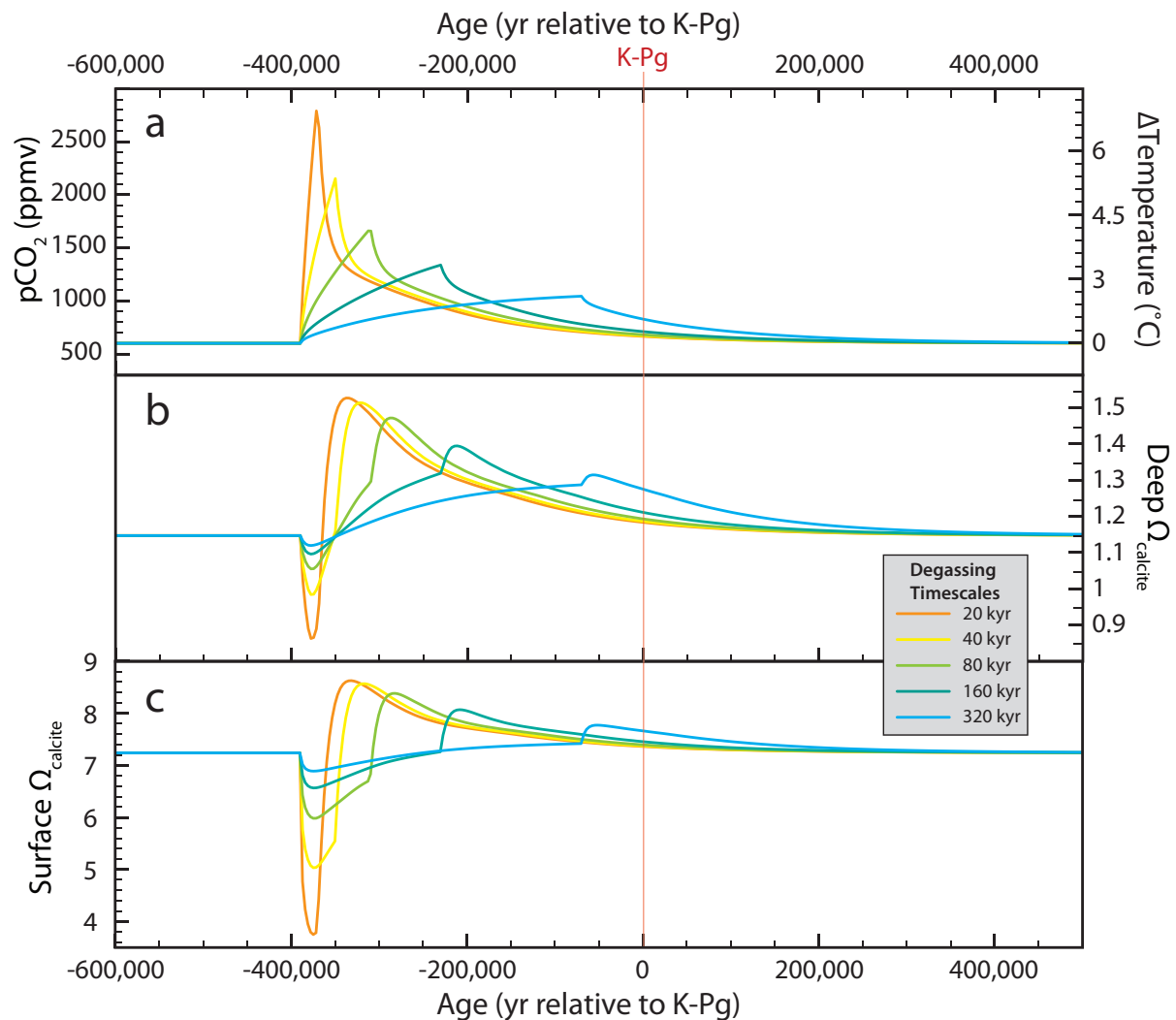


**Fig. S6:** Demonstration of different climate and carbonate-system responses to Deccan degassing according to the timescales of eruption. Note in these simulations the maximum total CO<sub>2</sub> and SO<sub>2</sub> emissions from Chenet et al.<sup>72</sup> are assumed (9,500 Gt C with 8,500 Gt S).

Recent palaeomagnetic work[67] has highlighted that within a broader window for the Phase II of Deccan emplacement, single eruptive events (SEEs) would have likely taken place on much shorter timescales, with hiatuses in between. To test whether more ‘pulsed’ patterns of emplacement substantially change the modeling conclusions drawn here, we divided the main eruptive pulse into 30 SEEs of 1kyr, distributed evenly over a 140 kyr timescale. While clearly the resultant simulation

results are spikier in trajectory, the resultant pCO<sub>2</sub> and ocean carbonate system changes after 140 kyr are unchanged (**Fig. S7**), and therefore our conclusions remain.

We note also that some of these records (the Southern Ocean and North Pacific sites in particular) suggest a possible second, shorter dissolution event somewhere between 100 and 160kyr before the K-Pg boundary (Fig. 1). A possible second pulse of Deccan perturbation has also recently been suggested in Tethyan sections by Thibault et al.[77]. It is possible that there is a second, true decline in terrestrially-derived Os isotopes that is not discernible in deep sea records due to overprinting from downcore leaching of extra-terrestrial Os[78]. Alternatively, if oceanic Os isotope change was driven more by fresh basalts obscuring a radiogenic craton source rock[79], as opposed to release of unradiogenic Os from fresh basalts[78,80], subsequent extrusions layering on top of existing basalts may not change Os isotope fluxes. That said, increase in sedimentary [Os] during the interval of decreasing <sup>187</sup>Os/<sup>188</sup>Os[2], and the unradiogenic <sup>187</sup>Os/<sup>188</sup>Os of Deccan source rocks[81] seem to implicate an influx of Deccan-sourced Os at this time rather than basalts merely obscuring a radiogenic Os source. In this case, one might expect continued evolution of seawater <sup>187</sup>Os/<sup>188</sup>Os with each addition of basalt (and hence Os). The evidence for a second dissolution event in our records is still equivocal and not consistent between sites, not least because distinguishing separate pulses of this resolution in the deep sea record becomes age-model dependent. Moreover, we note there is little suggestion of two separate warming events in records of δ<sup>18</sup>O (Fig. 1). Therefore, while we acknowledge this as a possibility, we refrain from distinguishing two pre-K-Pg pulses of emplacement here, pending further investigations. Some 'three pulse' scenarios were tested over the course of this study, and results are given in Supplementary Table 2.

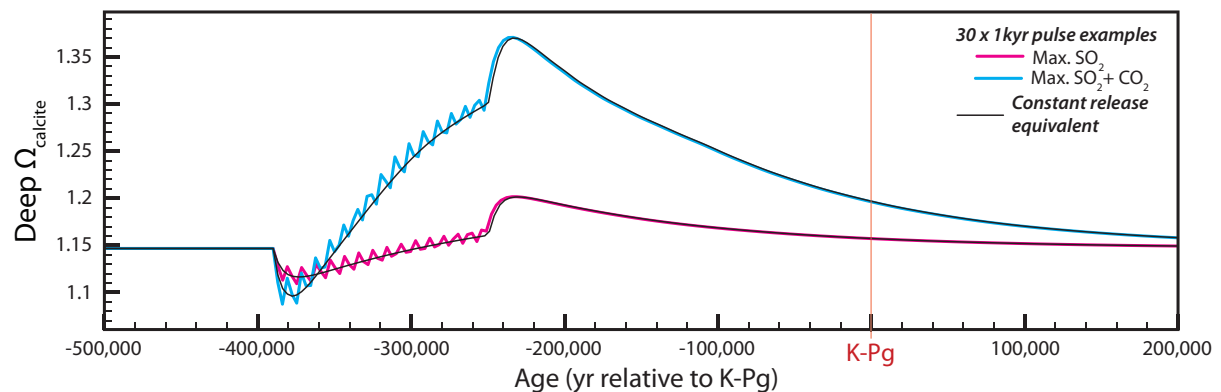


**Fig. S7:** To account for the likelihood of multiple brief single eruptive events (SEEs) within the second phase of Deccan emplacement<sup>72</sup>, eruptive scenarios were broken into 30 x 1kyr episodes, evenly spaced within a 140kyr window. While these runs are more irregular, there is little evidence in terms of long term trends between these runs (in colour, representative examples given here) and corresponding constant-release scenarios (black lines). Although SEEs were in reality unlikely to be evenly spaced in time, this would likely serve only to increase the irregularity of the trajectory, and would not dramatically change the overall effects of Deccan eruption.

Finally, it has also been suggested that fluxes of CO<sub>2</sub> from Deccan emplacement may have been accentuated through contact metamorphism of hydrocarbon-rich sediments[82]. While we cannot rule this out, minimal changes in marine δ<sup>13</sup>C records during the Maastrichtian portion of magnetochron C29r suggests this is unlikely to have played any role here, and as such we do not attempt to simulate this.

### 5c. Deccan Trap simulations: Extending dissolution and avoiding carbonate overshoot

There are two striking mismatches between modelled scenarios presented here (Fig. 3) and the sedimentary record (Fig. 1). Firstly, the timescales of dissolution suggested by deep ocean saturation decrease in LOSCAR are far shorter than the timescales for preservation change that are seen in sediments. Secondly, LOSCAR consistently suggests that the dominant signal of Deccan emplacement would be a rise in oceanic carbonate saturation due to silicate weathering feedbacks. Only one record, to our knowledge, could support a deepening of the CCD in response to Deccan degassing: that of the Ontong-Java plateau (ODP Site 803), where enhanced preservation at the K-Pg boundary was interpreted as beginning in the *M. prinsii* zone in the uppermost Maastrichtian[83]. This is an intriguing possibility, but in the absence of any signal of enhanced preservation in records

from elsewhere, remains an open question. Therefore both the extended dissolution and lack of obvious carbonate overshoot may invoke the existence some compensating feedback.

One proposed effect of LIP volcanism is an increased supply of P to the oceans, stimulating productivity<sup>e.g.</sup>[84]. Such an increase in primary productivity could act to negate at least some of the weathering-induced lysocline deepening, and perhaps extend dissolution intervals. However, we note that there is little evidence for enhanced productivity and export in the aftermath of Deccan volcanism in either benthic  $\delta^{13}\text{C}$ [11,12,85],  $\text{C}_{\text{org}}$  accumulation[85], or biogenic barium accumulation[47]. Nannofossil taxa at this time have in fact been interpreted as indicating increased oligotrophy[53,86], while there seems little in benthic foraminiferal assemblages to suggest an increase supply of food[e.g. 87,88].

An alternative mechanism, then, to enhance dissolution and avoid carbonate overshoot without substantial change in  $\delta^{13}\text{C}_{\text{DIC}}$  is to change the rain ratio of  $\text{CaCO}_3:\text{C}_{\text{org}}$  during Deccan warming. In the modern ocean, oligotrophy favours coccolithophore production over siliceous and organic-walled primary producers[e.g. 89]. If Deccan warming resulted in enhanced stratification and more oligotrophic oceans, as has been suggested[e.g. 90,86,53], it is likely that  $\text{CaCO}_3$  production and export rose. An increase in  $\text{CaCO}_3:\text{C}_{\text{org}}$  ratio of 30% during warming succeeds in extending the timescales of deep ocean dissolution to approximate agreement with sedimentary records, amplifying atmospheric  $\text{CO}_2$  rise, and in dampening subsequent carbonate saturation increase (**Fig. S8**). This places further emphasis on the importance of accounting for biotic feedbacks when considering the ocean's response to greenhouse gas forcings, both for past events and future projections.

Another means of reducing deep sea carbonate saturation without substantial change in  $\delta^{13}\text{C}_{\text{DIC}}$  is through an increase in  $\text{CaCO}_3$  deposition on shelves, as has been suggested for the MECO[91]. Certainly, there is potential for large-scale ocean saturation changes from even a ~ 20% shift in carbonate burial from deep ocean to shelf simulated in **Fig. S9**. Thermal expansion, and perhaps even loss of sea ice[92], could have caused minor transgression of continental seaways during Deccan eruptions, conceivably allowing more area for shelf deposition of  $\text{CaCO}_3$ . As yet, however, we are aware of little direct evidence for any such increased  $\text{CaCO}_3$  mass accumulation rates on shelf sections during this time, and so a role for shelf partitioning in muting carbonate overshoot is still speculative.

Besides biogeochemical feedbacks, there are possible limitations in our modelling approach that may contribute to data-model mismatch. For example, the limitations in spatial resolution and a lack of ocean currents in LOSCAR may make it impossible to reproduce the spatially and temporally heterogeneous patterns of carbonate preservation records. Alternatively, the lack any parameterisation of organic carbon respiration within sediments in LOSCAR may conceivably render sediments under-sensitive to dissolution. Finally, seawater chemistry in the Cretaceous, being lower in borate[93] and sulphate[94] may not be adequately represented in models whose dissolution kinetics and carbonate buffering calculations are tuned to modern seawater compositions. That said, changing the dissolution rate constant ( $K_{\text{sd}}$ ) and dissolution rate order ( $N_{\text{sd}}$ ), that translate deepwater  $\Omega$  to dissolution[55], does little to extend the timespan of dissolution (see Runs 159, 160, Table S1).

We note that changing the strength of the silicate weathering feedback ascribed in LOSCAR cannot resolve model-data mismatch. A lower silicate weathering feedback strength may extend deep ocean undersaturation to some degree (as plotted in **Fig. S10**), but the effect is still not sufficiently large to match sediment records, and would as a corollary mean that atmospheric  $\text{pCO}_2$  would not be drawn down to return to pre-eruption temperatures prior to the K-Pg, as proxy data suggest. A higher-than-modern weathering feedback, consistent with vast expanses of fresh basalt exposed at tropical latitudes, is more consistent with temperature records.

One final possibility is that the length of the Cretaceous portion of Chron 29r as assigned in GTS2012[20] (358 kyr), is too long. If our preservation records from Cretaceous C29r were in fact condensed into ~250 kyr (as in ref. [62]) or even ~150 kyr (as in ref. [95]), the disagreement between the model and data (in terms of duration of dissolution if not carbonate overshoot) disappears. While we do not attempt to argue here that these carbonate preservation data are justification for reassessing the geological timescale, recent absolute age estimates[62,95] do certainly suggest that there may be some case for a reappraisal.

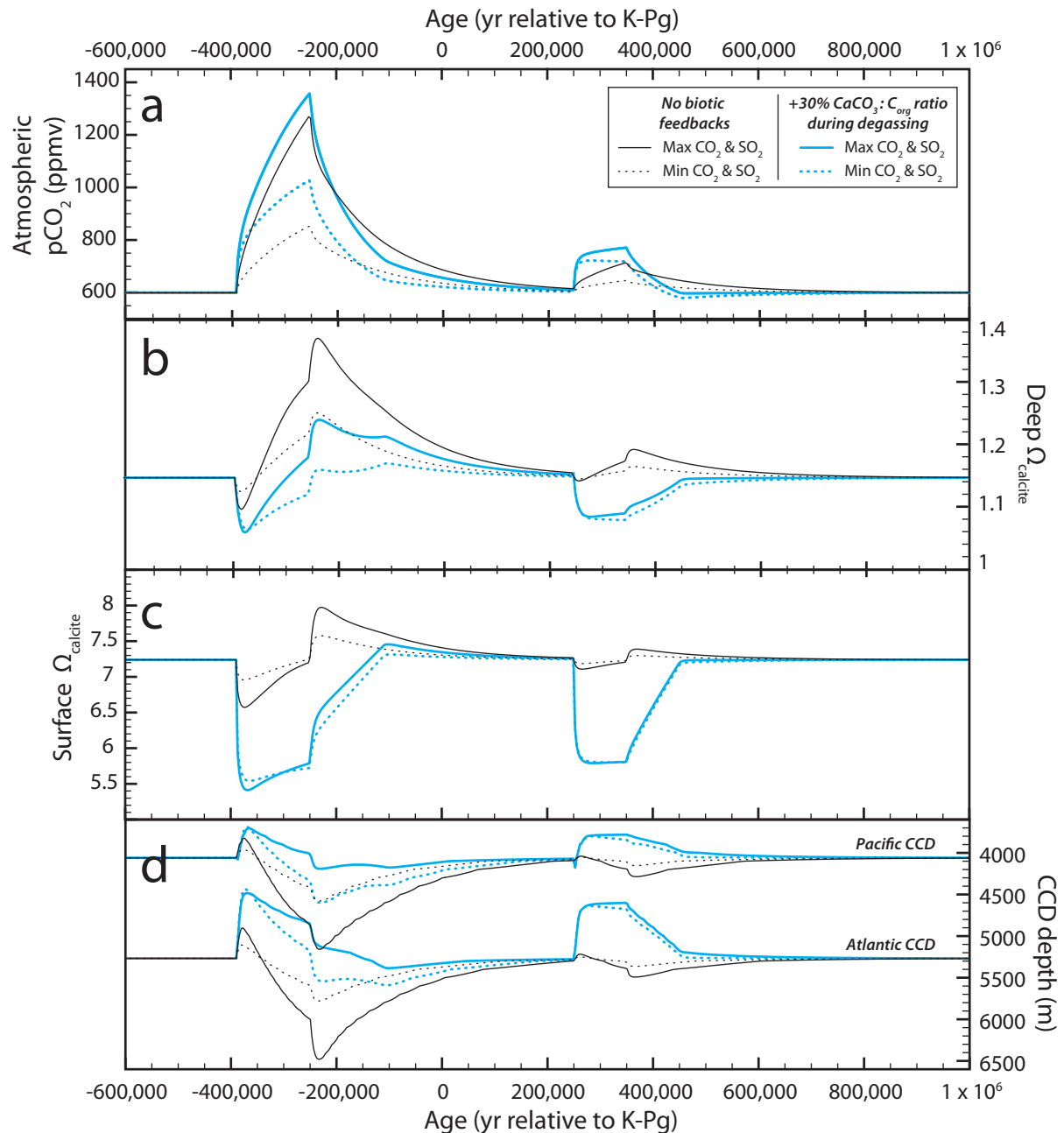


**Fig. S8:** Increasing the CaCO<sub>3</sub>:C<sub>org</sub> rain rate (blue) for the 140kyr duration of degassing (and linearly decreasing again over a further 140 kyr) results in higher atmospheric CO<sub>2</sub> concentration (Panel a), considerably less of a rise in oceanic saturation state (Panels b, c) and less of a CCD deepening (Panel d) than emissions scenarios where CaCO<sub>3</sub>:C<sub>org</sub> ratios are unchanged (black).

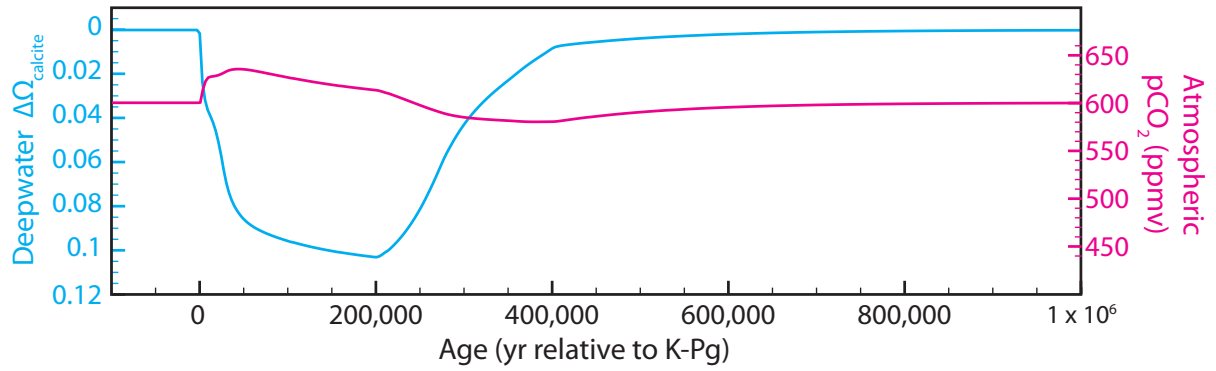


**Fig. S9:** Increasing partitioning of  $\text{CaCO}_3$  deposition towards the shelves (from 4.5 x pelagic rain rate to 6 x pelagic rain rate) reduces deep ocean saturation and thus shoals the CCD, making it a potential candidate for avoiding carbonate overshoot in the Maastrichtian, and ocean supersaturation in the early Danian.

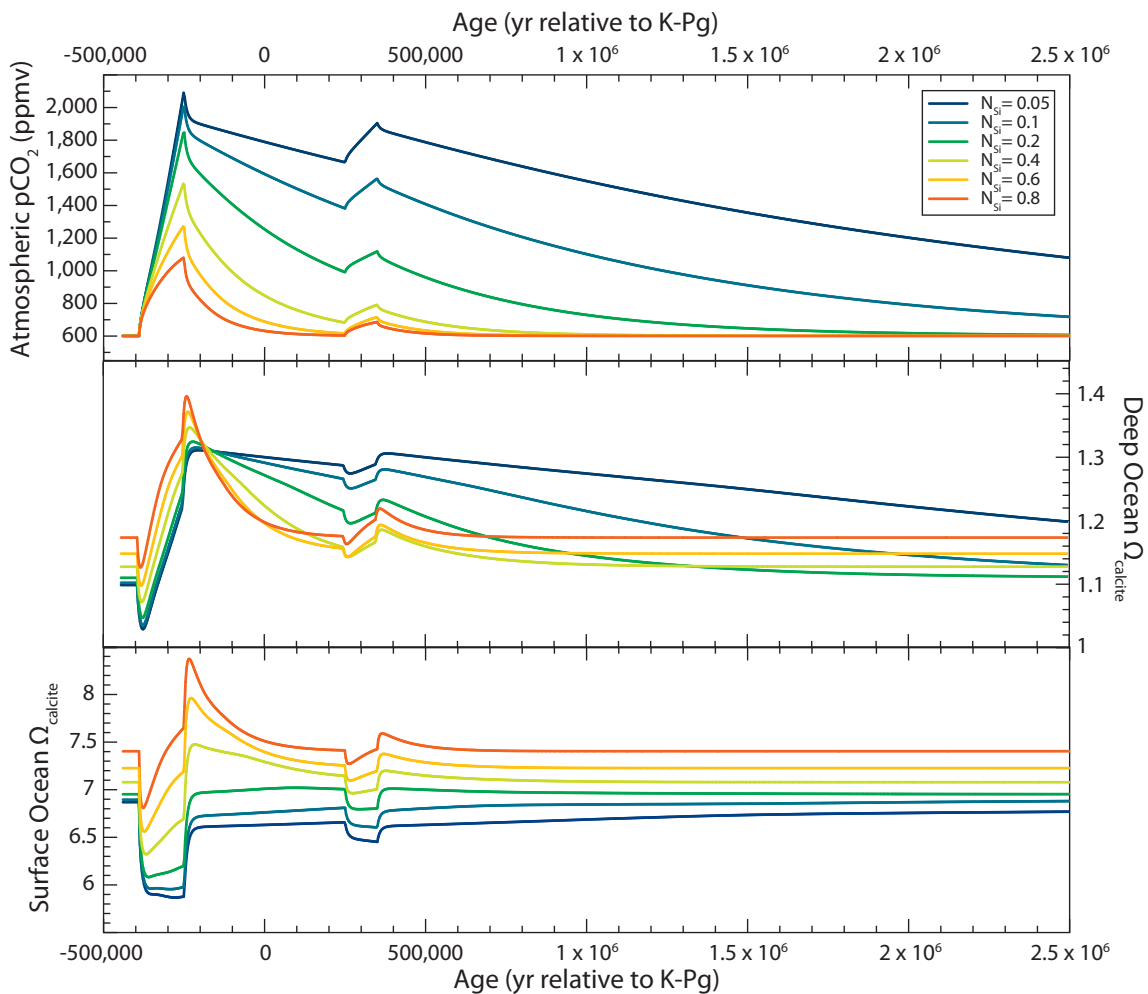


**Fig. S10:** Altering the strength of silicate weathering feedbacks in LOSCAR ( $N_{Si}$ ) will alter the trajectories of atmospheric  $p\text{CO}_2$  and oceanic calcite saturation state. However, no value for  $N_{Si}$  can reproduce prolonged dissolution and rapid  $p\text{CO}_2$  drawdown consistent with sedimentary records. Values for surface (0-100m) and deep (1,000 - 6,500 m)  $\Omega$  are for the average surface and deep Pacific boxes respectively.

#### 5d. K-Pg bolide aftermath

After bolide impact and the extinction of most pelagic calcifying species at the K-Pg boundary,  $\text{CaCO}_3$  export fluxes to deep ocean sediments were drastically reduced, perhaps by as much as a factor of four or more[48,96]. Caldeira et al.[97] first predicted using box modelling that such a reduction in pelagic  $\text{CaCO}_3$  production should have led to increased oceanic carbonate saturation, a deepening of the lysocline to the seafloor, and  $\text{CO}_2$  drawdown in the early Danian. To explain a lack of such a signal in sediments, they suggest that higher carbonate ion saturation and nutrient availability might have promoted  $\text{CaCO}_3$  production on the continental shelf that compensated for the loss of pelagic producers. Later, Caldeira and Rampino[98] suggested that a 25% increase in shelf  $\text{CaCO}_3$  deposition was sufficient to compensate.

There are a number of reasons for revisiting this problem here. Firstly, our more exhaustive collation of sedimentary evidence now indicates greatly increased oceanic saturation state at this time. Besides records of fragmentation shown in Fig. 2 and changes in CCD depth highlighted in the main text, there are many qualitative indicators for globally increased seawater  $\Omega$  in the Danian. At DSDP Site 239 in the Indian Ocean, planktic foraminifera are found in the Danian, where in the Maastrichtian there are none preserved[99]. Smit and Van Kempen[100] cite qualitatively enhanced preservation in the earliest Danian at DSDP Sites 47.2, 305, and 465 in the Pacific Ocean, and DSDP Sites 142, 365, and 524 in the Atlantic. In addition, an increase in ocean  $\Omega$  in the Danian is supported by a predominance of dissolution-susceptible coccoliths[49], enhanced preservation of microfossils at DSDP Sites 356[49] and 577[26], and high mass accumulation rates of intact minute foraminifera[10] (in the modern ocean, this small size class are often heavily dissolved within the water column[101]). These new records allow us to better constrain the true extent of CCD deepening after the K-Pg.

Secondly, LOSCAR is a model of greater complexity and spatial resolution than used previously, allowing us to better predict and compare CCD depth changes in different ocean basins. Finally, in previous models[97,98] the ratio of Mg to Ca in the Cretaceous oceans was taken to be similar to today, which we now know was highly unlikely[102–104]. This has implications not only for calculation of ocean saturation states in such a model, but also for the calculation of carbonate speciation, because of the importance of ion pairing in altering speciation constants ( $K_1$ ,  $K_2$ , etc.)[58]. As such, it is important to re-examine the validity of these previous studies according to our most up-to-date understanding.

Plotted in Fig. 3, we simulate the geologically instantaneous extinction of most pelagic calcifiers as a step change in the ratio of  $C_{\text{org}}:\text{CaCO}_3$  (i.e. keeping  $C_{\text{org}}$  flux constant but reducing  $\text{CaCO}_3$  flux by a set percentage). Note that in LOSCAR, pelagic  $\text{CaCO}_3$  export flux is parameterized as a function of  $C_{\text{org}}$  flux, which in turn is a function of nutrient availability[see 55]. This assumes that primary productivity in the oceans was unperturbed (globally, on geological timescales) by the K-Pg impact event[47,105,106]. However, if widespread collapsed surface-deep  $\delta^{13}\text{C}$  gradients are not solely the result of metabolic vital effects[106,107] in early Danian planktic foraminifera, there must also be some global reduction in  $C_{\text{org}}$  flux. To approximate this using LOSCAR, we reduce the efficiency of the biological pump, such that biota are less effective at utilizing the nutrient pool (in the case of LOSCAR, P being the critical determining nutrient). Both the  $\text{CaCO}_3$  rain reduction and the export efficiency changes are imposed for a period of 200 kyr, after which they are gradually returned to pre-event values over the course of a further 200 kyr to represent the gradual evolutionary recovery of nannofossil taxa.

As is clear from Figs. 3, S5 and S11, even 30 – 50% reduction in the rain ratio produces pronounced oversaturation of  $\text{CaCO}_3$  in the world's oceans. Were pelagic fluxes of  $\text{CaCO}_3$  to have been reduced by 50%, surface water  $\Omega_{\text{calcite}}$  would begin to approach a level of supersaturation ( $\Omega > 14$ ) whereby spontaneous abiotic precipitation of  $\text{CaCO}_3$  could begin (Fig. S11). A lack of widespread abiotic carbonate deposits in the early Danian suggests that these levels of carbonate saturation are improbable, although we note an increased abundance of carbonate macrocrystals in the earliest Danian[108] could be evidence for some abiotic precipitation, perhaps in the form of 'whittings'. LOSCAR also predicts that a 50% reduction in pelagic  $\text{CaCO}_3$  flux would have brought Pacific CCD depths down to ca. 6340 m, though, which is incompatible with a lack of carbonate preserved at IODP Site U1365 at this time (palaeodepth ca. 4,400)[109]. More compatible, though, is a 30% drop in  $\text{CaCO}_3$  export, which would lower the Pacific CCD to ~4200: enough to bring the CCD below IODP U1370 but remain above U1365, consistent with observations[109].

How then might these findings be reconciled with much larger decreases in pelagic  $\text{CaCO}_3$  mass accumulation observed in some deep sea sites (as much as 90% by some estimates)[48,96,110,111]? Although reducing the efficiency of the entire biological pump (i.e. the ability of both  $C_{\text{org}}$  and  $\text{CaCO}_3$  producers to exploit nutrients), rather than changing  $C_{\text{org}}:\text{CaCO}_3$  rain ratio, results in less pronounced oversaturation of the ocean (Fig. 3), this is in part an artefact of the

architecture of LOSCAR. In LOSCAR, when efficiency of the biological pump is lowered, nutrients (parameterized as P) accumulate in surface ocean boxes. This has the effect of compensating for some of the initial loss in productivity, since although the biological pump is less efficient at 'converting' nutrients to carbon export, the resulting larger nutrient reservoir dampens this forcing by promoting productivity. While in some senses this is perhaps a more realistic representation of a biological system, it is likely that in such a eutrophic system with excess nutrients, ecosystems would shift from the more 'k-strategist' calcareous nannoplankton, to more 'r-strategist'  $C_{org}$  producers[89] such as dinoflagellates: an ecological shift beyond the complexity of geochemical box-modeling. So while in LOSCAR an equal reduction in both  $CaCO_3$  and  $C_{org}$  are prescribed when changing the efficiency of the biological pump, in reality in the ocean such a situation might never arise. An increase in the export of  $C_{org}$  to the deep ocean following the K-Pg boundary could have conceivably reduced the extent of CCD deepening following the removal of pelagic carbonate producers. However, it is difficult to reconcile this with a rise in benthic foraminiferal  $\delta^{13}C$  widely observed after the K-Pg[e.g. 85,106], even if indeed some indicators do suggest at least regional increases in export productivity[47].

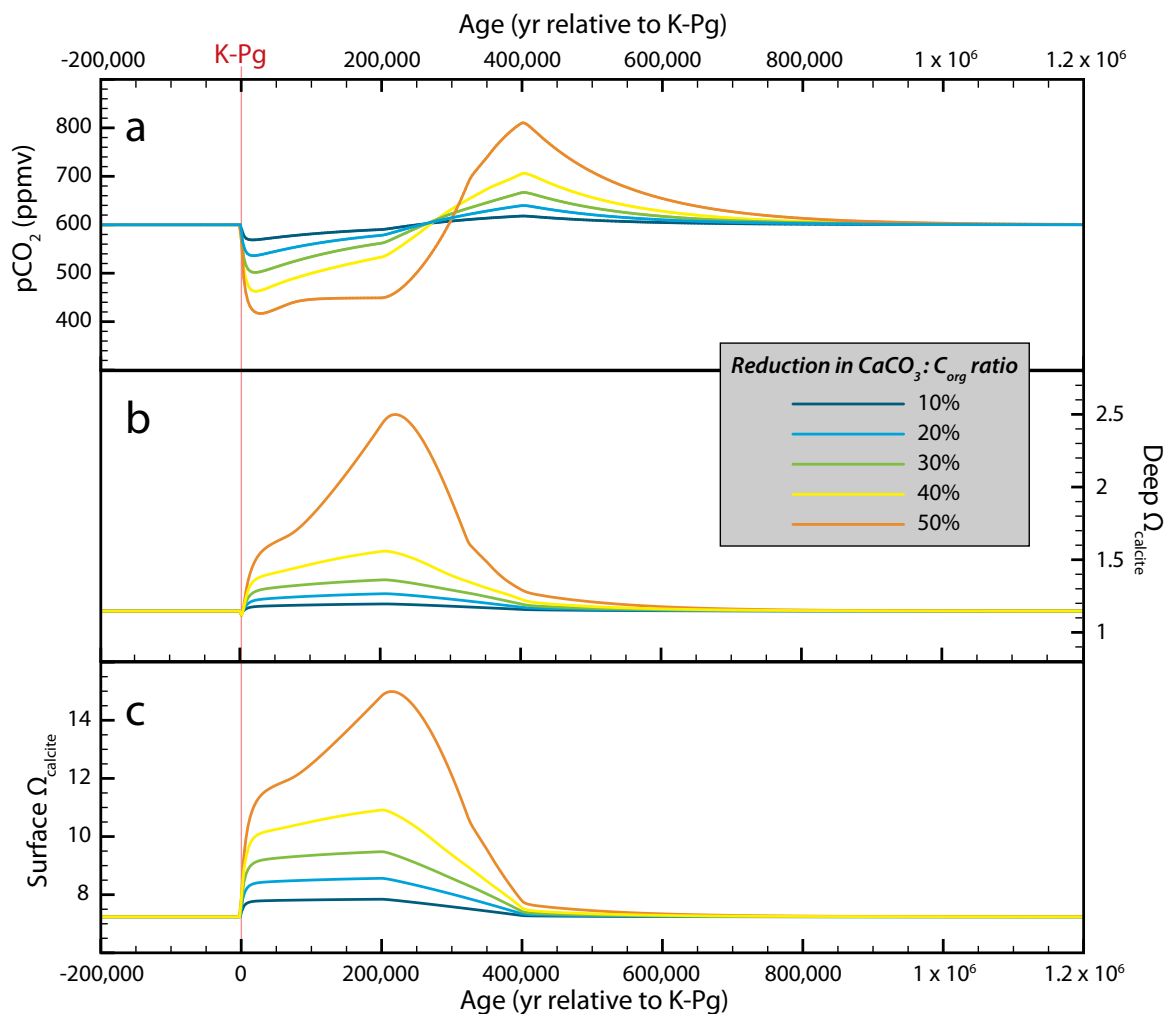


**Fig. S11:** Demonstration of the effects of different scenarios for the reduction of  $CaCO_3:C_{org}$  rain rate at the K-Pg boundary, following extinction of pelagic calcifiers. While a 30% reduction is permissible with current CCD constraints (see text), reductions of >50% are probably unfeasible. Reducing by >75%, as changes in deep see carbonate mass accumulation rates might suggest, would produce deep ocean saturations of >15, and atmospheric  $pCO_2$  of ~200 ppm. These simulations are clearly unreasonable and are not shown here. In all simulations, the change in  $CaCO_3:C_{org}$  rain rate is imposed for 200 kyr, and then returned to pre-event values gradually over a further 200 kyr.

As such, in the absence of alternative mechanisms, we echo previous studies[97,98] in concluding that if typical estimates of CaCO<sub>3</sub> mass accumulation rate reduction in the deep sea were indeed >> 30 % [6 and references within], LOSCAR would require carbon burial in shelf settings to have increased for the CCD not to have approached the seafloor (see Fig. S9, S11). Intuitively, higher partitioning of carbonate production toward the shelves seems probable, given the preferential survival of neritic nannofossil [10,50,112] and foraminiferal [113] taxa during the K-Pg mass extinction. The outstanding problem with such a mechanism, though, is that empirical estimates of early Danian sedimentation rates in shelf settings are either the same (Seymour Island, Antarctica [114]) or in fact lower (New Zealand [115,116], Tethyan sections [117], Northeast Atlantic [118] and Danish basin [105]) than during the Maastrichtian. Therefore a priority if we are to better understand carbon cycling in the aftermath of the K-Pg bolide impact is to ascertain whether (and where) any rise in shelf deposition took place, if there is some other mechanism that may have mitigated CCD deepening, or whether LOSCAR is instead prone in some way to overestimation of deep ocean carbonate saturation.

## 6. Literature Cited

1. Ehrendorfer, T. W. 1993 Late Cretaceous (Maestrichtian) Calcareous Nannoplankton Biogeography with Emphasis on Events Immediately Preceding the Cretaceous/Paleocene Boundary. PhD thesis, MIT/WHOI.
2. Robinson, N., Ravizza, G., Coccioni, R., Peucker-Ehrenbrink, B. & Norris, R. 2009 A high-resolution marine 187Os/188Os record for the late Maastrichtian: Distinguishing the chemical fingerprints of Deccan volcanism and the KP impact event. *Earth Planet. Sci. Lett.* **281**, 159–168. (doi:10.1016/j.epsl.2009.02.019)
3. O'Connell, S. B. 1990 Variations in Upper Cretaceous and Cenozoic Calcium Carbonate Percentages, Maud Rise, Weddell Sea, Antarctica. *Proc. Ocean Drill. Program Sci. Results* **113**, 971–984.
4. Norris, R. D. et al. 2014 U1403. In *Paleogene Newfoundland Sediment Drifts*, pp. 98 pp. College Station, TX: Integrated Ocean Drilling Program.
5. Kucera, M., Malmgren, B. A. & Stuessen, U. 1997 Foraminiferal dissolution at shallow depths of the Walvis Ridge and Rio Grande Rise during the latest Cretaceous: Inferences for deep-water circulation in the South Atlantic. *Palaeogeogr. Palaeoclimatol. Palaeoecol.* **129**, 195–212. (doi:10.1016/S0031-0182(96)00133-2)
6. D'Hondt, S. 2005 Consequences of the Cretaceous/Paleogene Mass Extinction for Marine Ecosystems. *Annu. Rev. Ecol. Evol. Syst.* **36**, 295–317. (doi:10.1146/annurev.ecolsys.35.021103.105715)
7. Hancock, H. J. L. & Dickens, G. R. 2005 Carbonate Dissolution Episodes in Paleocene and Eocene Sediment, Shatsky Rise, West-Central Pacific. *Proc. Ocean Drill. Program Sci. Results Leg* **198**.
8. Gerstel, J., Thunell, R. C., Zachos, J. C. & Arthur, M. A. 1986 The Cretaceous/Tertiary Boundary Event in the North Pacific: Planktonic foraminiferal results from Deep Sea Drilling Project Site 577, Shatsky Rise. *Paleoceanography* **1**, 97–117. (doi:10.1029/PA001i002p00097)
9. Zachos, J. C., Arthur, M. A. & Dean, W. E. 1989 Geochemical evidence for suppression of pelagic marine productivity at the Cretaceous/Tertiary boundary. *Nature* **337**, 61–64. (doi:10.1038/337061a0)
10. Hull, P. M., Norris, R. D., Bralower, T. J. & Schueth, J. D. 2011 A role for chance in marine recovery from the end-Cretaceous extinction. *Nat. Geosci.* **4**, 856–860. (doi:10.1038/ngeo1302)

11. Westerhold, T., Röhl, U., Donner, B., McCarren, H. K. & Zachos, J. C. 2011 A complete high-resolution Paleocene benthic stable isotope record for the central Pacific (ODP Site 1209). *Paleoceanography* **26**, PA2216. (doi:10.1029/2010PA002092)
12. Li, L. & Keller, G. 1998 Abrupt deep-sea warming at the end of the Cretaceous. *Geology* **26**, 995–998. (doi:10.1130/0091-7613(1998)026<0995:ADSWAT>2.3.CO;2)
13. D'Hondt, S. & Lindinger, M. 1994 A stable isotopic record of the Maastrichtian ocean-climate system: South Atlantic DSDP site 528. *Palaeogeogr. Palaeoclimatol. Palaeoecol.* **112**, 363–378. (doi:10.1016/0031-0182(94)90081-7)
14. Stott, L. D. & Kennett, J. P. 1990 The paleoceanographic and paleoclimatic signature of the Cretaceous/Paleogene boundary in the Antarctic: stable isotopic results from ODP Leg 113. In *Proceedings of the Ocean Drilling Project*, pp. 829–848. College Station, TX.
15. Kroon, D., Zachos, J. C. & Shipboard Scientific Party 2007 Leg 208 Synthesis: Cenozoic Climate Cycles and Excursions. In *Proceedings of the Ocean Drilling Program, Scientific Results* (eds D. Kroon J. C. Zachos & C. Richter), pp. 1–55. College Station, TX: IODP.
16. Shipboard Scientific Party 2002 Leg 198 Summary. In *Proceedings of the Ocean Drilling Project*, pp. 1–148. College Station, TX: Ocean Drilling Program.
17. Westerhold, T. & Röhl, U. 2006 Data report: Revised composite depth records for Shatsky Rise Sites 1209, 1210, and 1211. In *Proceedings of the Ocean Drilling Program, Scientific Results* (eds T. J. Bralower I. Premoli Silva & M. J. Malone), College Station, TX: Ocean Drilling Program.
18. Westerhold, T., Röhl, U., Raffi, I., Fornaciari, E., Monechi, S., Reale, V., Bowles, J. & Evans, H. F. 2008 Astronomical calibration of the Paleocene time. *Palaeogeogr. Palaeoclimatol. Palaeoecol.* **257**, 377–403. (doi:10.1016/j.palaeo.2007.09.016)
19. Westerhold, T., Röhl, U. & Laskar, J. 2012 Time scale controversy: Accurate orbital calibration of the early Paleogene. *Geochem. Geophys. Geosystems* **13**, 19 PP. (doi:10.1029/2012GC004096)
20. Gradstein, F. M., Ogg, J. G., Schmitz, M. & Ogg, G. 2012 *The Geologic Time Scale 2012 2-Volume Set*. Elsevier.
21. Barker, P. ., Kennett, J. P. & et al., editors 1988 *Proceedings of the Ocean Drilling Program, 113 Initial Reports*. Ocean Drilling Program. [cited 2015 Jul. 28].
22. Erez, J. & Luz, B. 1983 Experimental paleotemperature equation for planktonic foraminifera. *Geochim. Cosmochim. Acta* **47**, 1025–1031. (doi:10.1016/0016-7037(83)90232-6)
23. Hamilton, N. 1990 Mesozoic Magnetostratigraphy of Maud Rise, Antarctica. *Proc. Ocean Drill. Program Sci. Results* **113**, 255–260.
24. Michel, H. V., Asaro, F., Alvarez, W. & Alvarez, L. W. 1990 Geochemical studies of the Cretaceous/Tertiary boundary in ODP Holes 689B and 690C. *Proc. Ocean Drill. Program Sci. Results* **113**, 159–168.
25. Heath, G. R., Burckle, L. H. & et al. 1985 *Initial Reports of the Deep Sea Drilling Project, 86*. U.S. Government Printing Office. [cited 2015 Jul. 27].
26. Zachos, J. C., Arthur, M. A., Thunell, R. C., Williams, D. F. & Tappa, E. J. 1985 Stable Isotope and Trace Element Geochemistry of Carbonate Sediments across the Cretaceous/Tertiary Boundary at Deep Sea Drilling Project Hole 577, Leg 86. *Initial Rep. Deep Sea Drill. Proj.* **86**, 513–532.

27. Dickens, G. R. & Backman, J. 2013 Core alignment and composite depth scale for the lower Paleogene through uppermost Cretaceous interval at Deep Sea Drilling Project Site 577. *Newsl. Stratigr.* **46**, 47–68. (doi:10.1127/0078-0421/2013/0027)
28. Bleil, U. 1985 THE MAGNETOSTRATIGRAPHY OF NORTHWEST PACIFIC SEDIMENTS, DEEP-SEA DRILLING PROJECT LEG-86. *Initial Rep. Deep Sea Drill. Proj.* **86**, 441–458.
29. Chave, A. D. 1984 Lower Paleocene-Upper Cretaceous Magnetostratigraphy, Site 525, Site 527 and Site 529, Deep Sea Drilling Project Leg 74. *Initial Rep. Deep Sea Drill. Proj.* **74**, 525–531.
30. Alvarez, W., Arthur, M. A., Fischer, A. G., Lowrie, W., Napoleone, G., Silva, I. P. & Roggenthen, W. M. 1977 Upper Cretaceous–Paleocene magnetic stratigraphy at Gubbio, Italy V. Type section for the Late Cretaceous–Paleocene geomagnetic reversal time scale. *Geol. Soc. Am. Bull.* **88**, 383. (doi:10.1130/0016-7606(1977)88<383:UCMSAG>2.0.CO;2)
31. Coccioni, R., Ferraro, G., Giusberti, L., Lirer, F., Luciani, V., Marsili, A. & Spezzaferri, S. 2004 New insight on the late Cretaceous–Eocene foraminiferal record from the classical Bottaccione and Contessa pelagic Tethyan sections (Gubbio, central Italy): results from high-resolution study and a new sample preparation technique. In *Abstracts*, Florence.
32. Henriksson, A. S. 1993 Biochronology of the terminal Cretaceous calcareous nannofossil Zone of *Micula prinsii*. *Cretac. Res.* **14**, 59–68. (doi:10.1006/cre.1993.1005)
33. Gardin, S., Galbrun, B., Thibault, N., Coccioni, R. & Silva, I. P. 2012 Bio-magnetostratigraphy for the upper Campanian & Maastrichtian from the Gubbio area, Italy: new results from the Contessa Highway and Bottaccione sections. *Newsl. Stratigr.* (doi:10.1127/0078-0421/2012/0014)
34. Berger, W. H. 1970 Planktonic Foraminifera: Selective solution and the lysocline. *Mar. Geol.* **8**, 111–138. (doi:10.1016/0025-3227(70)90001-0)
35. Melguen, M. 1978 Facies evolution, carbonate dissolution cycles in sediments from the eastern south atlantic (DSDP Leg 40) since the early Cretaceous. *Initial Rep. Deep Sea Drill. Proj.* **60**, 543–586.
36. Berger, W. H., Bonneau, M.-C. & Parker, F. L. 1982 Foraminifera on the deep-sea floor: lysocline and dissolution rate. *Oceanol. Acta* **5**, 249–258. (doi:0399-1784/1982/249)
37. Malmgren, B. A. 1987 Differential dissolution of Upper Cretaceous planktonic foraminifera from a temperate region of the South Atlantic Ocean. *Mar. Micropaleontol.* **11**, 251–271. (doi:10.1016/0377-8398(87)90001-6)
38. Arrhenius, G. 1953 Sediment Cores from the East Pacific. *Geol. Foereningen Stockh. Foerhandlingar* **75**, 115–118. (doi:10.1080/11035895309454862)
39. Colosimo, A. B., Bralower, T. J. & Zachos, J. C. 2006 Evidence for lysocline shoaling at the Paleocene/Eocene Thermal Maximum on Shatsky Rise, northwest Pacific. In *Proceedings of the Ocean Drilling Project, Scientific Results* (eds T. J. Bralower I. Premoli Silva & M. J. Malone), pp. 1–36. College Station, TX.
40. Hayward, B. W., Carter, R., Grenfell, H. R. & Hayward, J. J. 2001 Depth distribution of Recent deep-sea benthic foraminifera east of New Zealand, and their potential for improving paleobathymetric assessments of Neogene microfaunas. *N. Z. J. Geol. Geophys.* **44**, 555–587. (doi:10.1080/00288306.2001.9514955)
41. Salgueiro, E. et al. 2008 Planktonic foraminifera from modern sediments reflect upwelling patterns off Iberia: Insights from a regional transfer function. *Mar. Micropaleontol.* **66**, 135–164. (doi:10.1016/j.marmicro.2007.09.003)

42. Le, J. & Shackleton, N. J. 1992 Carbonate Dissolution Fluctuations in the Western Equatorial Pacific During the Late Quaternary. *Paleoceanography* **7**, 21–42. (doi:10.1029/91PA02854)
43. Hull, P. M. et al. submitted Speeding up community morphometrics with open code and data sharing. *Methods Ecol. Evol.*
44. Thierstein, H. R. & Roth, P. H. 1991 Stable isotopic and carbonate cyclicity in Lower Cretaceous deep-sea sediments: Dominance of diagenetic effects. *Mar. Geol.* **97**, 1–34. (doi:10.1016/0025-3227(91)90017-X)
45. Schlanger, S. O. & Douglas, R. G. 1974 The pelagic ooze-chalk limestone transition and its implications for marine stratigraphy. In *Pelagic Sediments - on Land and Under the Sea (Special Publication 1 of the IAS)* (eds K. J. Hsü & H. C. Jenkyns), pp. 117–148. New York: John Wiley & Sons.
46. Haug, G. H. & Tiedemann, R. 1998 Effect of the formation of the Isthmus of Panama on Atlantic Ocean thermohaline circulation. *Nature* **393**, 673–676. (doi:10.1038/31447)
47. Hull, P. M. & Norris, R. D. 2011 Diverse patterns of ocean export productivity change across the Cretaceous-Paleogene boundary: New insights from biogenic barium. *Paleoceanography* **26**, PA3205. (doi:10.1029/2010PA002082)
48. Zachos, J. C. & Arthur, M. A. 1986 Paleoceanography of the Cretaceous/Tertiary Boundary Event: Inferences from stable isotopic and other data. *Paleoceanography* **1**, PP. 5–26. (doi:198610.1029/PA001i001p00005)
49. Thierstein, H. R. 1980 Selective dissolution of late cretaceous and earliest tertiary calcareous nanofossils: Experimental evidence. *Cretac. Res.* **1**, 165–176. (doi:10.1016/0195-6671(80)90023-3)
50. Thierstein, H. R. 1981 Late Cretaceous Nannoplankton and the Change at the Cretaceous-Tertiary Boundary. In *The Deep Sea Drilling Project: A Decade of Progress* (eds J. E. Warme R. G. Douglas & E. L. Winterer), pp. 355–394. Tulsa, Oklahoma: Society of Economic Palaeontologists and Mineralogists.
51. Peucker-Ehrenbrink, B. & Ravizza, G. 2000 The marine osmium isotope record. *Terra Nova* **12**, 205–219. (doi:10.1046/j.1365-3121.2000.00295.x)
52. Clement, B. M., Kent, D. V. & Opdyke, N. D. 1996 A synthesis of magnetostratigraphic results from Pliocene-Pleistocene sediments cored using the hydraulic piston corer. *Paleoceanography* **11**, 299–308. (doi:10.1029/95PA03524)
53. Thibault, N., Gardin, S. & Galbrun, B. 2010 Latitudinal migration of calcareous nanofossil *Micula murus* in the Maastrichtian: Implications for global climate change. *Geology* **38**, 203–206. (doi:10.1130/G30326.1)
54. Zeebe, R. E., Zachos, J. C. & Dickens, G. R. 2009 Carbon dioxide forcing alone insufficient to explain Palaeocene–Eocene Thermal Maximum warming. *Nat. Geosci.* **2**, 576–580. (doi:10.1038/ngeo578)
55. Zeebe, R. E. 2012 LOSCAR: Long-term Ocean-atmosphere-Sediment CARbon cycle Reservoir Model v2.0.4. *Geosci Model Dev* **5**, 149–166. (doi:10.5194/gmd-5-149-2012)
56. Ben-Yaakov, S. & Goldhaber, M. B. 1973 The influence of sea water composition on the apparent constants of the carbonate system. *Deep Sea Res. Oceanogr. Abstr.* **20**, 87–99. (doi:10.1016/0011-7471(73)90044-2)
57. Stanley, S. M. & Hardie, L. A. 1998 Secular oscillations in the carbonate mineralogy of reef-building and sediment-producing organisms driven by tectonically forced shifts in seawater

- chemistry. *Palaeogeogr. Palaeoclimatol. Palaeoecol.* **144**, 3–19. (doi:10.1016/S0031-0182(98)00109-6)
58. Hain, M. P., Sigman, D. M., Higgins, J. A. & Haug, G. H. 2015 The effects of secular calcium and magnesium concentration changes on the thermodynamics of seawater acid/base chemistry: Implications for Eocene and Cretaceous ocean carbon chemistry and buffering. *Glob. Biogeochem. Cycles*, 2014GB004986. (doi:10.1002/2014GB004986)
59. Millero, F. J. & Pierrot, D. 1998 A Chemical Equilibrium Model for Natural Waters. *Aquat. Geochem.* **4**, 153–199. (doi:10.1023/A:1009656023546)
60. Ridgwell, A. 2005 A Mid Mesozoic Revolution in the regulation of ocean chemistry. *Mar. Geol.* **217**, 339–357. (doi:10.1016/j.margeo.2004.10.036)
61. Chenet, A.-L., Quidelleur, X., Fluteau, F., Courtillot, V. & Bajpai, S. 2007 40K-40Ar dating of the Main Deccan large igneous province: Further evidence of KTB age and short duration. *Earth Planet. Sci. Lett.* **263**, 1–15. (doi:10.1016/j.epsl.2007.07.011)
62. Schoene, B., Samperton, K. M., Eddy, M. P., Keller, G., Adatte, T., Bowring, S. A., Khadri, S. F. R. & Gertsch, B. 2015 U-Pb geochronology of the Deccan Traps and relation to the end-Cretaceous mass extinction. *Science* **347**, 182–184. (doi:10.1126/science.aaa0118)
63. Dessert, C., Dupré, B., François, L. M., Schott, J., Gaillardet, J., Chakrapani, G. & Bajpai, S. 2001 Erosion of Deccan Traps determined by river geochemistry: impact on the global climate and the 87Sr/86Sr ratio of seawater. *Earth Planet. Sci. Lett.* **188**, 459–474. (doi:10.1016/S0012-821X(01)00317-X)
64. Uchikawa, J. & Zeebe, R. E. 2008 Influence of terrestrial weathering on ocean acidification and the next glacial inception. *Geophys. Res. Lett.* **35**, L23608. (doi:10.1029/2008GL035963)
65. Berner, R. A. 2004 *The Phanerozoic Carbon Cycle: CO<sub>2</sub> and O<sub>2</sub>*. Oxford: Oxford University Press.
66. Tyrrell, T., Merico, A. & Armstrong McKay, D. I. 2015 Severity of ocean acidification following the end-Cretaceous asteroid impact. *Proc. Natl. Acad. Sci.*, 201418604. (doi:10.1073/pnas.1418604112)
67. Chenet, A.-L., Courtillot, V., Fluteau, F., Gérard, M., Quidelleur, X., Khadri, S. F. R., Subbarao, K. V. & Thordarson, T. 2009 Determination of rapid Deccan eruptions across the Cretaceous-Tertiary boundary using paleomagnetic secular variation: 2. Constraints from analysis of eight new sections and synthesis for a 3500-m-thick composite section. *J. Geophys. Res. Solid Earth* **114**, B06103. (doi:10.1029/2008JB005644)
68. Intergovernmental Panel on Climate Change, editor 2014 *Climate Change 2013 - The Physical Science Basis: Working Group I Contribution to the Fifth Assessment Report of the Intergovernmental Panel on Climate Change*. Cambridge: Cambridge University Press. [cited 2015 Aug. 1].
69. Rogner, H., Aguilera, R. F., Archer, C. L., Bertani, R., Bhattacharya, S. C., Dusseault, M. B., Gagnon, L. & Yakushev, V. 2012 Energy Resources and Potentials. In *Global Energy Assessment - Toward a Sustainable Future* (eds T. B. Johansson A. Patwardhan N. Nakicenovic & L. Gomez-Echeverri), pp. 423–513. Cambridge, UK and New York, USA: Cambridge University Press.
70. Self, S., Widdowson, M., Thordarson, T. & Jay, A. E. 2006 Volatile fluxes during flood basalt eruptions and potential effects on the global environment: A Deccan perspective. *Earth Planet. Sci. Lett.* **248**, 518–532. (doi:10.1016/j.epsl.2006.05.041)

71. Jay, A. E. & Widdowson, M. 2008 Stratigraphy, structure and volcanology of the SE Deccan continental flood basalt province: implications for eruptive extent and volumes. *J. Geol. Soc.* **165**, 177–188. (doi:10.1144/0016-76492006-062)
72. Self, S., Widdowson, M., Thordarson, T. & Jay, A. E. 2006 Volatile fluxes during flood basalt eruptions and potential effects on the global environment: A Deccan perspective. *Earth Planet. Sci. Lett.* **248**, 518–532. (doi:10.1016/j.epsl.2006.05.041)
73. Caldeira, K. & Rampino, M. R. 1990 Carbon dioxide emissions from Deccan volcanism and a K/T boundary greenhouse effect. *Geophys. Res. Lett.* **17**, 1299–1302.
74. McLean, D. M. 1985 Deccan Traps Mantle Degassing in the Terminal Cretaceous Marine Extinctions. *Cretac. Res.* **6**, 235–259.
75. Kaminski, E., Chenet, A.-L., Jaupart, C. & Courtillot, V. 2011 Rise of volcanic plumes to the stratosphere aided by penetrative convection above large lava flows. *Earth Planet. Sci. Lett.* **301**, 171–178. (doi:10.1016/j.epsl.2010.10.037)
76. Nordt, L., Atchley, S. & Dworkin, S. I. 2002 Paleosol barometer indicates extreme fluctuations in atmospheric CO<sub>2</sub> across the Cretaceous–Tertiary boundary. *Geology* **30**, 703–706. (doi:10.1130/0091-7613(2002)030<0703:PBIEFI>2.0.CO;2)
77. Thibault, N., Galbrun, B., Gardin, S., Minoletti, F. & Le Callonnec, L. 2015 The end-Cretaceous in the southwestern Tethys (Elles, Tunisia): orbital calibration of paleoenvironmental events before the mass extinction. *Int. J. Earth Sci.* (doi:10.1007/s00531-015-1192-0)
78. Robinson, N., Ravizza, G., Coccioni, R., Peucker-Ehrenbrink, B. & Norris, R. 2009 A high-resolution marine 187Os/188Os record for the late Maastrichtian: Distinguishing the chemical fingerprints of Deccan volcanism and the KP impact event. *Earth Planet. Sci. Lett.* **281**, 159–168. (doi:10.1016/j.epsl.2009.02.019)
79. Ravizza, G. & Peucker-Ehrenbrink, B. 2003 Chemostratigraphic Evidence of Deccan Volcanism from the Marine Osmium Isotope Record. *Science* **302**, 1392–1395. (doi:10.1126/science.1089209)
80. Cohen, A. & Coe, A. 2002 New geochemical evidence for the onset of volcanism in the Central Atlantic magmatic province and the environmental change at the Triassic–Jurassic boundary. *Geology* **30**, 267–270.
81. Allègre, C. J., Birck, J. L., Capmas, F. & Courtillot, V. 1999 Age of the Deccan traps using 187Re–187Os systematics. *Earth Planet. Sci. Lett.* **170**, 197–204. (doi:10.1016/S0012-821X(99)00110-7)
82. Gilmour, I., Gilmour, M., Jolley, D., Kelley, S., Kemp, D., Daly, R. & Watson, J. 2013 A high-resolution nonmarine record of an early Danian hyperthermal event, Boltysh crater, Ukraine. *Geology* **41**, 783–786. (doi:10.1130/G34292.1)
83. Berger, W. H., Kroenke, L. W., Mayer, L. A., Backman, J., Janecek, T. R., Krissek, L., Leckie, M. & Lyle, M. 1992 The record of Ontong Java Plateau: Main results of ODP Leg 130. *Geol. Soc. Am. Bull.* **104**, 954–972. (doi:10.1130/0016-7606(1992)104<0954:TROOJP>2.3.CO;2)
84. Armstrong McKay, D. I., Tyrrell, T., Wilson, P. A. & Foster, G. L. 2014 Estimating the impact of the cryptic degassing of Large Igneous Provinces: A mid-Miocene case-study. *Earth Planet. Sci. Lett.* **403**, 254–262. (doi:10.1016/j.epsl.2014.06.040)
85. Esmeray-Senlet, S., Wright, J. D., Olsson, R. K., Miller, K. G., Browning, J. V. & Quan, T. M. 2015 Evidence for reduced export productivity following the Cretaceous/Paleogene mass extinction: Productivity after the K/Pg Boundary. *Paleoceanography*, n/a–n/a. (doi:10.1002/2014PA002724)

86. Thibault, N. & Gardin, S. 2010 The calcareous nannofossil response to the end-Cretaceous warm event in the Tropical Pacific. *Palaeogeogr. Palaeoclimatol. Palaeoecol.* **291**, 239–252.
87. Alegret, L. & Thomas, E. 2013 Benthic foraminifera across the Cretaceous/Paleogene boundary in the Southern Ocean (ODP Site 690): Diversity, food and carbonate saturation. *Mar. Micropaleontol.* **105**, 40–51. (doi:10.1016/j.marmicro.2013.10.003)
88. Alegret, L. & Thomas, E. 2007 Deep-Sea environments across the Cretaceous/Paleogene boundary in the eastern South Atlantic Ocean (ODP Leg 208, Walvis Ridge). *Mar. Micropaleontol.* **64**, 1–17. (doi:10.1016/j.marmicro.2006.12.003)
89. Cermeno, P., Dutkiewicz, S., Harris, R. P., Follows, M., Schofield, O. & Falkowski, P. G. 2008 The role of nutricline depth in regulating the ocean carbon cycle. *Proc. Natl. Acad. Sci.* **105**, 20344–20349. (doi:10.1073/pnas.0811302106)
90. Thibault, N. & Gardin, S. 2007 The late Maastrichtian nannofossil record of climate change in the South Atlantic DSDP Hole 525A. *Mar. Micropaleontol.* **65**, 163–184. (doi:10.1016/j.marmicro.2007.07.004)
91. Sluijs, A., Zeebe, R. E., Bijl, P. K. & Bohaty, S. M. 2013 A middle Eocene carbon cycle conundrum. *Nat. Geosci.* **6**, 429–434. (doi:10.1038/ngeo1807)
92. Bowman, V. C., Francis, J. E. & Riding, J. B. 2013 Late Cretaceous winter sea ice in Antarctica? *Geology* **41**, 1227–1230. (doi:10.1130/G34891.1)
93. Lemarchand, D., Gaillardet, J., Lewin, É. & Allègre, C. J. 2002 Boron isotope systematics in large rivers: implications for the marine boron budget and paleo-pH reconstruction over the Cenozoic. *Chem. Geol.* **190**, 123–140. (doi:10.1016/S0009-2541(02)00114-6)
94. Lowenstein, T. K., Timofeeff, M. N., Brennan, S. T., Hardie, L. A. & Demicco, R. V. 2001 Oscillations in Phanerozoic Seawater Chemistry: Evidence from Fluid Inclusions. *Science* **294**, 1086–1088.
95. Sprain, C. J., Renne, P. R., Wilson, G. P. & Clemens, W. A. 2015 High-resolution chronostratigraphy of the terrestrial Cretaceous-Paleogene transition and recovery interval in the Hell Creek region, Montana. *Geol. Soc. Am. Bull.* **127**, 393–409. (doi:10.1130/B31076.1)
96. D'Hondt, S., Herbert, T. D., King, J. & Gibson, C. 1996 Planktic foraminifera, asteroids, and marine production: Death and recovery at the Cretaceous-Tertiary boundary. In *Special Paper 307: The Cretaceous-Tertiary Event and Other Catastrophes in Earth History*, pp. 303–317. Geological Society of America. [cited 2015 Jun. 5].
97. Caldeira, K., Rampino, M. R., Volk, T. & Zachos, J. C. 1990 Biogeochemical modeling at mass extinction boundaries: Atmospheric carbon dioxide and ocean alkalinity at the K/T boundary. In *Extinction Events in Earth History* (eds E. G. Kauffman & O. H. Walliser), pp. 333–345. Berlin/Heidelberg: Springer-Verlag. [cited 2015 Jun. 17].
98. Caldeira, K. & Rampino, M. R. 1993 Aftermath of the end-Cretaceous mass extinction: Possible biogeochemical stabilization of the carbon cycle and climate. *Paleoceanography* **8**, 515–525. (doi:10.1029/93PA01163)
99. Schlich, R. et al. 1974 Site 239. In *Initial Reports of the Deep Sea Drilling Project, 25* (eds E. S. W. Simpson R. Schlich & et al.), pp. 25–63. U.S. Government Printing Office. [cited 2015 Jun. 17].
100. Smit, J. & van Kempen, T. M. G. 1986 Planktonic foraminifers from the Cretaceous/Tertiary boundary at Deep Sea Drilling Project site 605, North Atlantic. In (eds J. E. Van Hinte & W. Wise), pp. 549–553. Washington D.C.: Deep Sea Drilling Project.

101. Ridgwell, A. J. & Zeebe, R. E. 2005 The role of the global carbonate cycle in the regulation and evolution of the Earth system. *Earth Planet. Sci. Lett.* **234**, 299–315. (doi:10.1016/j.epsl.2005.03.006)
102. Tyrrell, T. & Zeebe, R. E. 2004 History of carbonate ion concentration over the last 100 million years. *Geochim. Cosmochim. Acta* **68**, 3521–3530. (doi:10.1016/j.gca.2004.02.018)
103. Coggon, R. M., Teagle, D. A. H., Smith-Duque, C. E., Alt, J. C. & Cooper, M. J. 2010 Reconstructing Past Seawater Mg/Ca and Sr/Ca from Mid-Ocean Ridge Flank Calcium Carbonate Veins. *Science* **327**, 1114–1117. (doi:10.1126/science.1182252)
104. Evans, D., Müller, W., Oron, S. & Renema, W. 2013 Eocene seasonality and seawater alkaline earth reconstruction using shallow-dwelling large benthic foraminifera. *Earth Planet. Sci. Lett.* **381**, 104–115. (doi:10.1016/j.epsl.2013.08.035)
105. Sepúlveda, J., Wendler, J. E., Summons, R. E. & Hinrichs, K.-U. 2009 Rapid Resurgence of Marine Productivity After the Cretaceous-Paleogene Mass Extinction. *Science* **326**, 129–132. (doi:10.1126/science.1176233)
106. Alegret, L., Thomas, E. & Lohmann, K. C. 2012 End-Cretaceous marine mass extinction not caused by productivity collapse. *Proc. Natl. Acad. Sci.* **109**, 728–732. (doi:10.1073/pnas.1110601109)
107. Thomas, E. 2007 Cenozoic mass extinctions in the deep sea: What perturbs the largest habitat on Earth? In *Special Paper 424: Large Ecosystem Perturbations: Causes and Consequences*, pp. 1–23. Geological Society of America. [cited 2014 Jul. 18].
108. Minoletti, F., de Rafelis, M., Renard, M., Gardin, S. & Young, J. 2005 Changes in the pelagic fine fraction carbonate sedimentation during the Cretaceous-Paleocene transition: contribution of the separation technique to the study of Bidart section. *Palaeogeogr. Palaeoclimatol. Palaeoecol.* **216**, 119–137. (doi:10.1016/j.palaeo.2004.10.006)
109. D'Hondt, S., Inagaki, F., Alvarez-Zarikian, C. A. & Expedition 329 Scientists 2011 South Pacific Gyre Subseafloor Life. *Proc. Integr. Ocean Drill. Program* **329**. (doi:http://dx.doi.org/10.2204/iodp.proc.329.2011)
110. Herbert, T. D. & D'Hondt, S. L. 1990 Precessional climate cyclicity in Late Cretaceous—Early Tertiary marine sediments: a high resolution chronometer of Cretaceous-Tertiary boundary events. *Earth Planet. Sci. Lett.* **99**, 263–275. (doi:10.1016/0012-821X(90)90115-E)
111. Rea, D. K., Dehn, J., Driscoll, N. W., Farrell, J. W., Janecek, T. R., Owen, R. M., Pospichal, J. J. & Resiwati, P. 1990 Paleooceanography of the eastern Indian Ocean from ODP Leg 121 drilling on Broken Ridge. *Geol. Soc. Am. Bull.* **102**, 679–690. (doi:10.1130/0016-7606(1990)102<0679:POTEIO>2.3.CO;2)
112. Bown, P. 2005 Selective calcareous nannoplankton survivorship at the Cretaceous-Tertiary boundary. *Geology* **33**, 653–656. (doi:10.1130/G21566AR.1)
113. Ashkenazi-Polivoda, S., Rak, C., Almogi-Labin, A., Zsolt, B., Ovadia, O. & Abramovich, S. 2014 Paleoecology of the K-Pg mass extinction survivor *Guembelitra* (Cushman): Isotopic evidence from pristine foraminifera from Brazos River, Texas (Maastrichtian). *Paleobiology* **40**, 24–33. (doi:10.1666/13317)
114. Tobin, T. S., Ward, P. D., Steig, E. J., Olivero, E. B., Hilburn, I. A., Mitchell, R. N., Diamond, M. R., Raub, T. D. & Kirschvink, J. L. 2012 Extinction patterns,  $\delta^{18}\text{O}$  trends, and magnetostratigraphy from a southern high-latitude Cretaceous–Paleogene section: Links with Deccan volcanism. *Palaeogeogr. Palaeoclimatol. Palaeoecol.* **350–352**, 180–188. (doi:10.1016/j.palaeo.2012.06.029)

115. Vajda, V. & Raine, J. I. 2003 Pollen and spores in marine Cretaceous/Tertiary boundary sediments at mid-Waipara River, North Canterbury, New Zealand. *N. Z. J. Geol. Geophys.* **46**, 255–273. (doi:10.1080/00288306.2003.9515008)
116. Strong, C. P. 2000 Cretaceous-Tertiary foraminiferal succession at Flaxbourne River, Marlborough, New Zealand. *N. Z. J. Geol. Geophys.* **43**, 1–20. (doi:10.1080/00288306.2000.9514867)
117. Mukhopadhyay, S., Farley, K. A. & Montanari, A. 2001 A Short Duration of the Cretaceous-Tertiary Boundary Event: Evidence from Extraterrestrial Helium-3. *Science* **291**, 1952–1955. (doi:10.1126/science.291.5510.1952)
118. Mary, C., Moreau, M.-G., Orue-Etxebarria, X., Apellaniz, E. & Courtillot, V. 1991 Biostratigraphy and magnetostratigraphy of the Cretaceous/Tertiary Sopelana section (Basque country). *Earth Planet. Sci. Lett.* **106**, 133–150. (doi:10.1016/0012-821X(91)90068-S)